IEEE Access
Multidisciplinary | Rapid Review | Open Access Journal

Received February 2, 2021, accepted February 7, 2021, date of publication February 10, 2021, date of current version February 19, 2021.

Digital Object Identifier 10.1109/ACCESS.2021.3058575

INVITED PAPER

Highly Sensitive Reflective-Mode Phase-Variation Permittivity Sensor Based on a Coplanar Waveguide Terminated With an Open Complementary Split Ring Resonator (OCSRR)

LIJUAN SU[1], (Member, IEEE), JONATHAN MUÑOZ-ENANO[1], (Graduate Student Member, IEEE), PARIS VÉLEZ[1], (Member, IEEE), MARTA GIL-BARBA[2], (Member, IEEE), PAU CASACUBERTA[1], AND FERRAN MARTIN[1], (Fellow, IEEE)

[1]GEMMA/CIMITEC, Departament d'Enginyeria Electrònica, Universitat Autònoma de Barcelona, 08193 Bellaterra, Spain
[2]Departamento Ingeniería Audiovisual y Comunicaciones, Universidad Politécnica de Madrid, 28031 Madrid, Spain.

Corresponding author: Lijuan Su (lijuan.su@uab.cat)

This work was supported in part by the Ministerio de Ciencia e Innovación (MICINN)-Spain under Grant TEC2016-75650-R and Grant PID2019-103904RB-I00, in part by the Generalitat de Catalunya under Grant 2017SGR-1159, in part by the Institució Catalana de Recerca i Estudis Avançats (who awarded Ferran Martín), in part by the European Regional Development Fund (ERDF), in part by the Secreteraria d'Universitats i Recerca (Gen. Cat.), and in part by the European Social Fund for the FI grant. The work of Paris Vélez and Lijuan Su was supported by the Juan de la Cierva Program under Grant IJCI-2017-31339 and Grant IJC2019-040786-I.

ABSTRACT This paper presents a one-port reflective-mode phase-variation microwave sensor consisting of a coplanar waveguide (CPW) transmission line terminated with a grounded open complementary split ring resonator (OCSRR). The sensor is useful for measuring the dielectric constant of the so-called material under test (MUT), which should be placed in contact with the OCSRR, the sensitive element. The output variable is the phase of the reflection coefficient. Design guidelines for the implementation of highly sensitive sensors are derived in the paper, and validated through simulation and experiment. As compared to other reflective-mode phase-variation sensors based on open-ended sensing lines, the designed and fabricated devices exhibit a very small sensitive region by virtue of the use of an electrically small resonant element, the OCSRR. The relevant figure of merit, defined as the ratio between the maximum sensitivity and the size of the sensing area (expressed in terms of the squared wavelength), is as high as FoM $= 5643°/\lambda^2$ in one of the reported prototypes. Moreover, the paper analyzes the effects of losses. From this study, it is concluded that MUT losses do not significantly affect the output variable, provided losses are small. It is also demonstrated that the sensor is useful to estimate the loss tangent of the considered MUT samples.

INDEX TERMS Coplanar waveguide (CPW), dielectric characterization, microwave sensor, open complementary split ring resonator (OCSRR), phase-variation sensor, reflective-mode sensor.

I. INTRODUCTION

One-port reflective-mode phase-variation sensors are very interesting devices for material characterization, including solid and liquids [1], [2]. Such sensors are especially useful for determining the dielectric constant of the so-called material under test (MUT), as well as other variables related to it, including material composition (e.g., solute content in diluted solutions), or defect detection, among others.

The main advantage of phase-variation sensors over microwave sensors based on frequency variation [3]–[11] and frequency splitting [12]–[18] concerns single frequency operation. Namely, phase-variation sensors can be designed in order to operate at a single frequency, thereby reducing the costs of the associated electronics, needed for the

The associate editor coordinating the review of this manuscript and approving it for publication was Derek Abbott.

generation of the interrogation signal. By contrast, frequency-variation and frequency-splitting sensors intrinsically require wideband signals for sensing (in a real scenario, such signals should be generated by means of expensive broadband voltage-controlled oscillators –VCOs). Coupling-modulation sensors operating at a single frequency have also been reported [19]–[29]. However, the phase is, in general, more robust against the effects of noise and electromagnetic interferences than the magnitude of the transmission coefficient (the typical output variable in coupling modulation sensors). Moreover, the phase is less sensitive to the effects of sensor losses and the presence of connectors, which are typically needed for sensing.

Additionally, one-port reflective-mode sensors are typically simpler than sensors operating in transmission, where at least a pair of ports is required for sensor implementation (two and four ports are needed in differential-mode reflection and transmission sensors, respectively [30]–[41]). Reflective-mode sensors are of special interest for liquid characterization based on submersing the sensitive part of the sensor in the MUT liquid [42].

The reflective-mode phase-variation sensors reported in [1], [2] are implemented in planar technology, thereby representing a good solution in terms of cost. Moreover, fully planar structures can be implemented in flexible substrates (thus opening the path to the implementation of conformal sensors [43], [44] and wearable sensors [45]), and are compatible with other technologies, e.g., microfluidics [4], [18], [33], [36], [46]–[49], lab-on-a-chip [50], etc. Most planar reflective-mode phase-variation sensors are based on open-ended transmission lines [1], [2], and are devoted to the characterization of solid or liquid samples (excellent sensitivities are reported in [1]). An exception is the phase-variation sensor presented in [51], which is applied to the measurement of small displacements between a movable slab and the static part of the sensor (the open-ended line). Phase-variation sensors based on electrically small single resonant elements (the sensitive part) have also been reported, but in such sensors the focus is the measurement of spatial variables [52], [53] (other sensors based on chains of resonant elements acting as electro-inductive-wave transmission lines, which also exploit phase-variation, have been recently reported [40]).

In this paper, reflective-mode phase-variation microwave sensors devoted to material characterization, where the sensing element is an electrically small planar resonator, are presented. Specifically, the considered resonant element is an open complementary split ring resonator (OCSRR), first reported in [54]. The paper shows that by terminating a coplanar waveguide (CPW) transmission line with a grounded OCSRR, very high sensitivity in the phase of the reflection coefficient (the output variable) with the dielectric constant of the MUT (the input variable) is achievable. To do so, the characteristic impedance and the electrical length of the CPW transmission line, as well as the quality factor of the OCSRR, must be adequately chosen. The paper provides design guidelines for that purpose. Such design guidelines are inferred from an exhaustive analysis of the sensor, based on the circuit schematic.

Indeed, the reported OCSRR-terminated CPW sensor is similar to previous reflective-mode phase-variation sensors where the sensing element is a low-impedance half-wavelength open-ended line cascaded to a high-impedance quarter-wavelength transmission line (or a cascade of high/low impedance quarter-wavelength transmission line sections) [1], [2]. Indeed, a grounded OCSRR behaves similar to an open-ended half-wavelength transmission line in the vicinity of resonance [55], and therefore a similar behavior is expected. However, by replacing the 180° line with an OCSRR, significant size reduction in the sensing area is achieved. This constitutes the main advantage of the proposed sensor. Nevertheless, the equivalence between both sensors (the one based on the OCSRR, presented in this work for the first time, and the one based on a half-wavelength open-ended sensing line), is exhaustively analyzed.

The paper is organized as follows: the proposed sensor topology, working principle, as well as the equivalent circuit model of the CPW terminated with a grounded OCSRR are reported in Section II. Based on this circuit model, a sensitivity analysis of the proposed OCSRR-based sensors is carried out in Section III, where the link to the sensors based on a half-wavelength open-ended sensing line is also included. Sensor validation through simulation and experiment is the subject of Section IV, which includes a comparison with the equivalent sensors based on half-wavelength open-ended sensing lines. The effects of losses are discussed in Section V, where a method to estimate the loss tangent of the MUT is also included. Section VI is devoted to the comparison of the proposed sensors to other phase-variation microwave sensors reported in the literature. Finally, the main conclusions are highlighted in Section VII.

II. THE PROPOSED OCSRR-BASED REFLECTIVE-MODE PHASE-VARIATION SENSOR, WORKING PRINCIPLE, AND CIRCUIT MODEL

In a recent paper [1], it was demonstrated that high-impedance quarter-wavelength or low-impedance half-wavelength open-ended sensing lines are useful for the implementation of highly sensitive reflective-mode phase-variation dielectric constant sensors. Moreover, it was shown that the sensitivity, defined as the derivative of the phase of the reflection coefficient (the output variable) with the dielectric constant of the MUT, can be further enhanced by cascading quarter-wavelength transmission line sections with alternating high/low characteristic impedance to the sensing line. The specific topology/schematic of such sensors for half-wavelength sensing line is depicted in Fig. 1. It is important to mention that the sensing region in the sensor of Fig. 1 is restricted to the half-wavelength open-ended sensing line. That is, sensitivity enhancement by cascading high/low impedance 90° transmission line sections entails an overall increase of the sensor size, but such sensitivity improvement

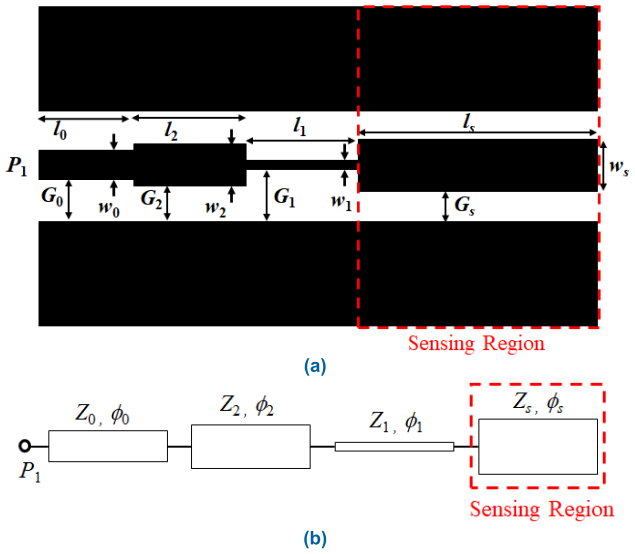

FIGURE 1. Typical topology (a) and schematic (b) of the one-port reflective-mode phase-variation sensor based on a step-impedance CPW configuration and a 180° open-ended sensing line. The sensing region is indicated with a dashed rectangle. For the topology, a pair of high/low impedance 90° line sections are considered. The electrical and geometrical variables are indicated, where the sub-index s refers to the sensing line, the numerical sub-indexes 1 and 2 denote the 90° line sections, and the numerical sub-index 0 corresponds to the access line.

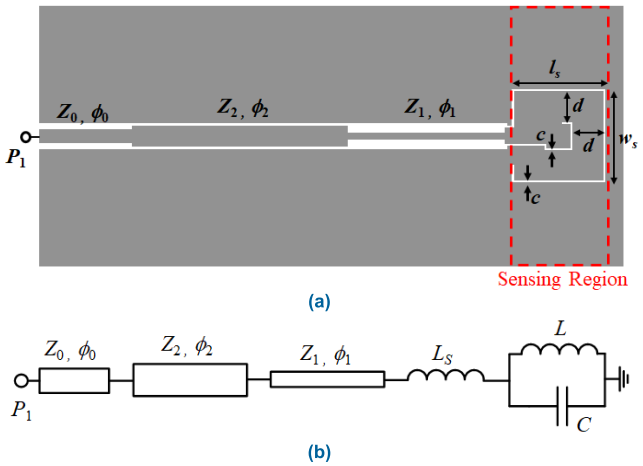

FIGURE 2. Typical topology (a) and circuit model (b) of the one-port reflective-mode phase-variation sensor based on a step-impedance CPW configuration terminated with an OCSRR, the sensing element. The sensing region is indicated with a dashed rectangle. For the topology, a pair of high/low impedance 90° line sections are considered. The relevant dimension variables of the OCSRR are indicated. The dimensions of the 90° lines are designated by the same variables as in Fig. 1. For the simulations referred to in the text, the dimensions of the OCSRR (in mm) are: $w_s = 10$, $l_s = 10$, $c = 0.2$, $d = 3.3$.

does not imply increasing the sensing region dimensions (unlike most phase-variation sensors [30], [32], [38], [40], [41], [56], [57]). Nevertheless, the size of the sensitive region, dictated by the length of the open-ended sensing line, cannot be considered to be small, especially in the case of the 180° sensing line sensor.

Based on the similar behavior between an open-ended half-wavelength transmission line and a grounded parallel resonator, the objective of this work is to replace the low-impedance 180° open-ended sensing line of the sensors reported in [1], [2] with a semi-lumped (i.e., electrically small) planar resonator that can be described (to a good approximation) by a parallel resonant tank. The expected result is a reflective-mode phase-variation sensor with behavior, in terms of performance, similar to the one of the sensors based on a purely distributed approach (Fig. 1), but with substantially reduced sensing area. This is an important aspect, since, for certain applications, the size of the MUT may be limited. For example, for liquid characterization, small amounts of MUT are typically available. This applies to submersible sensors, a canonical application of reflective-mode sensors [42], and also to microfluidic-based sensors [4], [18], [33], [36], [46]–[49] (in this latter case, the sensitive region must be covered by the fluidic channel, containing the liquid under test). However, small sensitive regions are also convenient for the characterization of solids, in order to reduce the size of the MUTs (this may have direct impact on cost reduction).

Among the semi-lumped planar resonators, probably the most interesting candidate for the implementation of the intended sensors is the so-called open complementary split ring resonator (OCSRR) [54]. The main reason is that this resonator is electrically very small (by virtue of its topology, as discussed in [54], [58]). Moreover, the sensor to be designed will be implemented in CPW technology, and therefore vias are not required for OCSRR grounding (nevertheless, as it will be shown, vias are needed to suppress the parasitic slot mode, since the OCSRR is not a symmetric resonator). The typical topology and circuit model of these OCSRR-terminated CPW transmission line sensors are depicted in Fig. 2 (note that the step-impedance discontinuities are considered to be ideal, i.e., not modelled by any equivalent circuit model). Other CPW sensors based on terminated CPWs are reported in [59], [60], whereas [61] reports a CSRR-loaded CPW transmission mode sensor, but devoted to the measurements of rotation and proximity.

The working principle of the sensor of Fig. 2 is very similar to the one of the purely distributed counterparts (Fig. 1). In brief, the presence of a MUT on top of the OCSRR modifies the capacitance of such element, and consequently the phase of the reflection coefficient seen from the plane of the particle also varies. Then, by virtue of the multiplicative effect of the step-impedance transmission line configuration (cascaded to the sensing element) on the variation of the phase of the reflection coefficient (seen from the input port) with the capacitance of the OCSRR, the sensitivity can be unprecedentedly enhanced [1].

Concerning the circuit model, it has been demonstrated that a microstrip line loaded with a shunt-connected OCSRR can be adequately, and accurately, described by means of a pure parallel resonant tank [62]. However, the precise description of the OCSRR-terminated CPW requires the presence of an additional series inductance, L_s, as depicted in Fig. 2. The inductance L_s is, indeed, a parasitic of the model, but it does

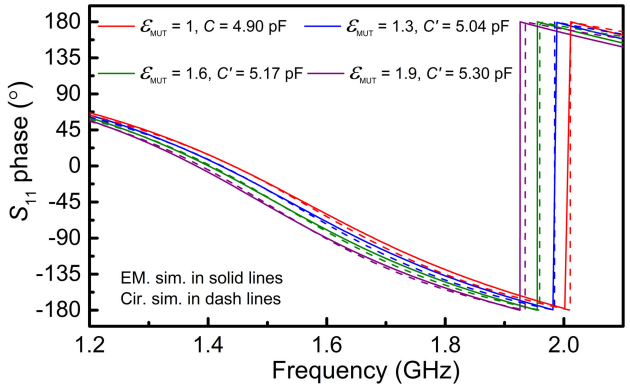

FIGURE 3. Phase of the reflection coefficient of the OCSRR-terminated CPW structure of Fig. 2, excluding the cascaded step-impedance CPW transmission line sections and access lines. The different curves correspond to the uncovered OCSRR (with capacitance $C = 4.90$ pF), and to the OCSRR covered with various semi-infinite MUTs with the indicated dielectric constant and capacitance, $C' = C + \Delta C$. The inductances in all the cases are $L = 2.48$ nH and $L_s = 2.63$ nH. The capacitances for the different considered MUTs obtained from the resonance frequency of the OCSRR of the EM. simulation, where the phase is null, are $C' = 5.04$ pF (for $\varepsilon_{MUT} = 1.3$), $C' = 5.19$ pF (for $\varepsilon_{MUT} = 1.6$), and $C' = 5.35$ pF (for $\varepsilon_{MUT} = 1.9$).

not jeopardize the performance of the sensor, as it will be demonstrated. Thus, the intrinsic reactive elements of the OCSRR are the capacitance C and the inductance L, and the element subjected to changes caused by the MUT is the capacitance C.

To validate the model of the OCSRR-terminated CPW, we have extracted the reactive parameters from the simulated phase of the reflection coefficient corresponding to the structure shown in Fig. 2, but excluding the high/low impedance 90° CPW line sections and access lines (the dimensions of the OCSRR are indicated in the caption). Moreover, the OCSRR is considered to be surrounded by air. The considered substrate is the *Rogers RO3010* with dielectric constant $\varepsilon_r = 10.2$ and thickness $h = 1.27$ mm (losses are excluded in the simulation). The simulated phase of the reflection coefficient, inferred from *Keysight Momentum*, is depicted in Fig. 3. It can be observed that the phase of the reflection coefficient reaches the value $-\pi$ at a finite frequency, designated as f_z. At such frequency, the impedance seen from the input port of the OCSRR-terminated CPW nulls. Consequently, the structure cannot be described merely by means of a grounded parallel LC resonant tank. A series inductance, L_s, is required to compensate the negative reactance of the OCSRR at f_z (note that at the OCSRR resonance, f_0, the impedance seen from the input port is an open-circuit, and above f_0 the reactance of the OCSRR is negative). Obviously, the reflection coefficient at f_0 exhibits a 0° phase, corresponding to an open-circuit. According to the circuit model, these relevant (and easily identifiable) frequencies are given by:

$$f_0 = \frac{1}{2\pi\sqrt{LC}} \tag{1}$$

$$f_z = \frac{1}{2\pi}\sqrt{\frac{1}{LC} + \frac{1}{L_s C}} \tag{2}$$

Expressions (1) and (2) are two conditions which are necessary to determine the reactive parameters of the circuit model of the OCSRR-terminated CPW transmission line. Nevertheless, an additional condition is required in order to univocally infer the three unknowns, L, C and L_s. Such condition may be, for instance, the phase at a certain arbitrary frequency in the region of interest. Alternatively, the three elements can be inferred by means of expressions (1) and (2), providing a unique degree of freedom, and curve fitting. This has been the considered procedure. Application of this parameter extraction method to the phase response of Fig. 3, has provided the reactive parameters indicated in the caption of such figure. The excellent agreement between the phases inferred from full-wave electromagnetic simulation and circuit simulation with the extracted parameters validates the proposed model, as well as the parameter extraction method.

For further validation of the model, the reflection coefficient of the OCSRR-terminated CPW of Fig. 2 has been simulated by considering that the OCSRR is covered by semi-infinite (in the vertical direction) MUTs of different dielectric constants. The effect is an increase in the capacitance of the OCSRR, determined by the dielectric constant of the MUT, $\varepsilon_{\mathrm{MUT}}$, according to [10]

$$C' = C + \Delta C = C\frac{\varepsilon_r + \varepsilon_{\mathrm{MUT}}}{\varepsilon_r + 1} \tag{3}$$

The validity of expression (3) is also restricted to substrate thicknesses significantly larger than the width of the slots of the OCSRR (the case in the present study). The simulated phase responses for the different MUTs are also included in Fig. 3, where the dielectric constants and the capacitances inferred from (3) are indicated. Note that the capacitances of the OCSRR covered with the different considered MUTs, C', can also be obtained from the resonance frequency (where the phase is null), provided neither L nor L_s are perturbed by the MUT. The capacitance values inferred from this procedure, included in the caption of Fig. 3, are in good agreement with those inferred from (3). From the capacitance values inferred by means of (3), the resulting phases obtained from circuit simulation are also depicted in Fig. 3. The good agreement between the circuit and electromagnetic simulations for the different values of $\varepsilon_{\mathrm{MUT}}$ validates the model of the OCSRR-terminated CPW, the dependence of the OCSRR capacitance on $\varepsilon_{\mathrm{MUT}}$, given by (3), as well as the parameter extraction procedure.

III. SENSITIVITY ANALYSIS

The main objective in the present paper is to implement highly sensitive dielectric constant sensors based on the OCSRR-CPW configuration shown in Fig. 2. Therefore, a sensitivity analysis based on the validated circuit model is pertinent, in order to infer design guidelines that link the required (maximum) sensitivity to the parameters of the model. Nevertheless, let us first consider only the OCSRR-terminated CPW. The generalization to the complete

sensor structure, also including the step-impedance CPW line sections, is very simple, as will be shown below (such step-impedance configuration has a multiplicative effect on the sensitivity, dictated by the impedance contrast of the different transmission line sections).

A. OCSRR-TERMINATED CPW

Let us call the impedance seen from the input port of the OCSRR-terminated CPW transmission line Z_{in}. The reflection coefficient seen from that port, with reference impedance Z_0, is simply [55]

$$\rho = \frac{Z_{\text{in}} - Z_0}{Z_{\text{in}} + Z_0} = \frac{j\chi_{\text{in}} - Z_0}{j\chi_{\text{in}} + Z_0} \tag{4}$$

χ_{in} being the input reactance. Thus, the phase of the reflection coefficient, the output variable, is given by

$$\phi_\rho = 2\arctan\left(-\frac{\chi_{\text{in}}}{Z_0}\right) + \pi \tag{5}$$

The input variable, ε_{MUT}, modifies the capacitance of the OCSRR, see expression (3), which, in turn, perturbs the reactance of the structure, χ_{in}. Thus, the sensitivity can be expressed as

$$S = \frac{d\phi_\rho}{d_{\varepsilon_{\text{MUT}}}} = \frac{d\phi_\rho}{dC'} \cdot \frac{dC'}{d_{\varepsilon_{\text{MUT}}}} = \frac{d\phi_\rho}{d\Delta C} \cdot \frac{d\Delta C}{d\varepsilon_{\text{MUT}}} \tag{6}$$

where $\Delta C = C' - C$ is the variation of the capacitance of the OCSRR when it is covered by a certain MUT (i.e., $\Delta C = 0$ for $\varepsilon_{\text{MUT}} = \varepsilon_{\text{MUT,air}} = 1$).

For the OCSRR-terminated CPW described by the circuit model of Fig. 2, excluding the different CPW line sections, the reactance and the phase of the reflection coefficient can be expressed as

$$\chi_{\text{in}} = \omega\left\{L_s + L\left[1 - \frac{\omega^2}{\omega_0^2}\left(1 + \frac{\Delta C}{C}\right)\right]^{-1}\right\} \tag{7}$$

and

$$\phi_\rho = 2\arctan\left\{-\frac{\omega}{Z_0}\left\{L_s + L\left[1 - \frac{\omega^2}{\omega_0^2}\left(1 + \frac{\Delta C}{C}\right)\right]^{-1}\right\}\right\} \tag{8}$$

respectively, where $\Omega = 2\pi f$ is the angular frequency, and $\Omega_0 = 2\pi f_0$ is the resonance (angular) frequency of the uncovered OCSRR, see expression (1). From (8), the first term of the sensitivity, $d\phi_\rho/d\Delta C$, can be calculated, i.e.,

$$\frac{d\phi_\rho}{d\Delta C} = \frac{-2}{1 + \frac{\chi_{\text{in}}^2}{Z_0^2}} \cdot \frac{L\omega^3}{CZ_0\omega_0^2} \cdot \frac{1}{\left[1 - \frac{\omega^2}{\omega_0^2}\left(1 + \frac{\Delta C}{C}\right)\right]^2} \tag{9}$$

Let us now assume that the interest is the optimization of the sensitivity in the vicinity of the dielectric constant of air ($\varepsilon_{\text{MUT}} = 1$), i.e., at $\Delta C = 0$. Evaluation of (9) when $\Delta C = 0$ gives

$$\left.\frac{d\phi_\rho}{d\Delta C}\right|_{\Delta C=0} \equiv S_{\Delta C}|_{\Delta C=0} = \frac{-2Z_0L\omega^3/C\omega_0^2}{\left(Z_0^2 + L_S^2\omega^2\right)\left(1 - \frac{\omega^2}{\omega_0^2}\right)^2 + 2LL_S\omega^2\left(1 - \frac{\omega^2}{\omega_0^2}\right) + L^2\omega^2} \tag{10}$$

Note that sensitivity optimization in the vicinity of $\varepsilon_{\text{MUT}} = 1$ does not represent a loss of generality. Namely, if the interest is to maximize the sensitivity for a different (arbitrary) value of ε_{MUT}, it suffices to obtain the capacitance of the OCSRR when it is covered with an MUT with such dielectric constant value, and the corresponding resonance frequency. In particular, it is possible to optimize the sensitivity in the vicinity of the dielectric constants of liquids, or other high dielectric constant materials (examples of highly sensitive sensors devoted to liquid characterization, based on different principles, have been reported [63], [64]).

Given a set of reactive parameters of the OCSRR-terminated CPW (L, C and L_s), the sensitivity in the limit of small perturbations ($\Delta C = 0$) depends on the operating frequency. In order to find the frequency that maximizes the sensitivity, it is necessary to derive $S_{\Delta C}|_{\Delta C=0}$ with frequency, and force the result to be zero. After a straightforward (but cumbersome) calculation, the following equation results:

$$-3L_s^2\frac{\omega^6}{\omega_0^4} + \left(2LL_s + 2L_s^2 - \frac{Z_0^2}{\omega_0^2}\right)\frac{\omega^4}{\omega_0^2} + \left[(L + L_s)^2 - 2\frac{z_0^2}{\omega_0^2}\right]\omega^2 + 3Z_0^2 = 0 \tag{11}$$

Finding the value of Ω in the previous equation is not easy (nevertheless, it is apparent that $\Omega = \omega_0$ is not a solution). Since the inductance L_s is a parasitic of the model, let us neglect it in (11). The resulting equation is found to be biquadratic in the variable Ω, and it can be expressed as

$$\frac{\omega^4}{\omega_0^4} + \left(2 - \frac{\omega_0'^2}{\omega_0^2}\right)\frac{\omega^2}{\omega_0^2} - 3 = 0 \tag{12}$$

where the following frequency variable has been defined in order to simplify the notation

$$\omega_0'^2 = \frac{Z_0^2}{L^2} \tag{13}$$

The solution of (12) is

$$\frac{\omega^2}{\omega_0^2} = -1 + \frac{1}{2}\frac{\omega_0'^2}{\omega_0^2} + 2\sqrt{1 + \frac{1}{4}\left(\frac{1}{4}\frac{\omega_0'^4}{\omega_0^4} - \frac{\omega_0'^2}{\omega_0^2}\right)} \tag{14}$$

Inspection of (14) reveals that if $\omega_0^2/\omega_0'^2 \ll 1$, the solution is $\omega \approx \omega_0$. In other words, for $\omega_0^2/\omega_0'^2 \ll 1$ and L_s negligible, the sensitivity in the limit of small perturbations

is optimized by setting the operating frequency of the sensor to roughly Ω_0, the resonance frequency of the bare OCSRR. From (10), the sensitivity of ϕ_ρ with ΔC, at $\Delta C = 0$ and $\Omega = \omega_0$, is found to be:

$$\left.\frac{d\phi_\rho}{d\Delta C}\right|_{\Delta C=0,\omega_0} \equiv \left. S_{\Delta C}\right|_{\Delta C=0,\omega_0} = -2Z_0\omega_0 \tag{15}$$

It can be seen that (15) does not depend on L_s, namely, we can neglect the effects of the parasitic inductance, L_s, provided the sensors is tuned to Ω_0. The whole sensitivity at this frequency, in the limit of small perturbations, can be calculated according to (6), where the first term is given by (15), and the second term can be easily obtained from (3), i.e.,

$$\frac{d\Delta C}{d\varepsilon_{\rm MUT}} = \frac{C}{\varepsilon_r + 1} \tag{16}$$

Therefore,

$$S|_{\Delta C=0,\omega_0} \equiv \left.\frac{d\phi_\rho}{d\varepsilon_{\rm MUT}}\right|_{\Delta C=0,\omega_0} = \frac{-2Z_0\omega_0 C}{\varepsilon_r + 1} \tag{17}$$

From (17), it follows that, in order to optimize the sensitivity, C should be high and, consequently, L must be low, so that the product LC is coherent with the frequency of operation $\omega_0 = 2\pi f_0 = 1/\sqrt{LC}$. According to the definition of Ω_0 and Ω_0', the squared ratio of these angular frequencies is

$$\frac{\omega_0^2}{\omega_0^2} = \frac{L}{CZ_0^2} = \frac{4}{\pi^2}\frac{Z_S^2}{Z_0^2} \tag{18}$$

where the equivalent impedance of the OCSRR resonator, defined as (see Appendix A)

$$Z_s = \frac{\pi}{2}\sqrt{\frac{L}{C}} \tag{19}$$

has been used. Note that the requirement of a high value of C and a low value of L for sensitivity optimization (or, equivalently, a low equivalent impedance, Z_s), is consistent with $\Omega\omega_0^2/\omega_0'^2 < 1$. Therefore, tuning the intrinsic resonance frequency of the OCSRR to Ω_0 with a high value of its capacitance C (and a low value of L) is a good strategy for sensitivity optimization. Moreover, at such frequency, the effects of L_s on the sensitivity for small perturbations are null, as demonstrated before.

Nevertheless, L_s is a parameter difficult to control in practice, and it is not necessarily very small as compared to L (see, e.g., the reactive parameters of the sensor structure of Fig. 2, indicated in the caption of Fig. 3). Under these conditions (i.e., if L_s cannot be neglected), it is not obvious that the optimum frequency for sensitivity enhancement is roughly Ω_0. To gain insight on this aspect, and due to the complexity of expression (11), where the dependence on L_s is not omitted, we have numerically solved such expression for different values of L_s and the values of L and C given in the caption of Fig. 3, with $Z_0 = 50\ \Omega$ (the usual reference impedance of the ports). The results, depicted in Fig. 4, indicate that

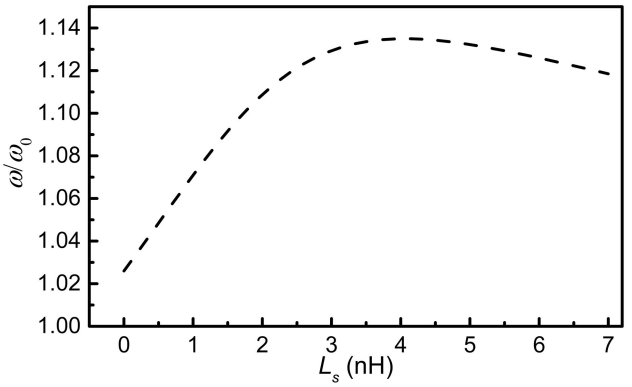

FIGURE 4. Dependence of the normalized optimum frequency, ω/ω_0, with L_s, as derived from the numerical solution of (11).

for low values of L_s, as compared to L, the optimum frequency approaches Ω_0, as expected. As L_s increases, the optimum frequency progressively diverges from Ω_0. For the specific value of L_s corresponding to the OCSRR-terminated structure under study ($L_s = 2.63$ nH), the optimum frequency is close to Ω_0 (i.e., 1.123 Ω_0, according to Fig. 4). From this study, it can be concluded that it is convenient to tune the operating frequency of the sensor to Ω_0. Such frequency is very close to the optimum one, and the sensitivity for small perturbations can be easily predicted, i.e., it is given by (17). Moreover, at ω_0, the parasitic inductance L_s, a parameter difficult to control, does not affect the sensitivity.

B. STEP-IMPEDANCE CPW CASCADED TO THE OCSRR-TERMINATED CPW

Let us now analyze the effects of a cascaded step-impedance CPW transmission line to the OCSRR-terminated structure. As it was demonstrated in [1], in reference to dielectric constant reflective-mode phase-variation sensors based on open-ended low-impedance 180° and high-impedance 90° sensing lines, the phase of the high/low transmission line sections must be 90° (or an odd multiple) for sensitivity optimization. Due to the similar behavior between an open-ended 180° line and a parallel LC resonator (see Appendix A, where it is demonstrated that both structures are equivalent in the vicinity of resonance), it follows that such phase condition (90°) should also be preserved for the high/low impedance sections of the step-impedance CPW structure in the considered sensor.

The impedance seen from the input port of the structure, consisting of N high/low impedance 90° line sections, plus the OCSRR-terminated CPW sensing structure, can be expressed as

$$Z_{{\rm in},N} = Z_{\rm in}^{(-1)^N} \cdot \prod_{i=1}^{N} \left\{ Z_i^{2\cdot(-1)^{i+N}} \right\} \tag{20}$$

where Z_i is the characteristic impedance of line section i (with $i = 1, 2, \ldots N$), and Π denotes the product operator. Thus,

the reflection coefficient can be expressed as

$$\rho = \frac{j(-1)^N \cdot \chi_{\text{in}}^{(-1)^N} \cdot \prod_{i=1}^{N} \left\{ Z_i^{2\cdot(-1)^{i+N}} \right\} - Z_0}{j(-1)^N \cdot \chi_{\text{in}}^{(-1)^N} \cdot \prod_{i=1}^{N} \left\{ Z_i^{2\cdot(-1)^{i+N}} \right\} + Z_0} \tag{21}$$

and the phase of the reflection coefficient is

$$\phi_\rho = 2\text{arctan}\left(-\frac{\chi_{\text{in}}}{\frac{Z_0}{\prod_{i=1}^{N} \left\{ Z_i^{2\cdot(-1)^{i+N}} \right\}}} \right) \tag{22a}$$

For N even, and

$$\phi_\rho = 2\text{arctan}\left(-\frac{\chi_{\text{in}}}{\frac{\prod_{i=1}^{N} \left\{ Z_i^{2\cdot(-1)^{i+N}} \right\}}{Z_0}} \right) \tag{22b}$$

for N odd. By comparing expressions (22) and (5), it follows that the phases are identical, except the denominator of the argument of the arctan. However, the single difference is a constant factor that depends on the impedances, Z_i, of the different line sections. Thus, the sensitivity for the OCSRR-based structure with cascaded high/low impedance 90° line sections is given by expression (17) by replacing Z_0 with the denominators of expressions (22) for each case, N even or odd, i.e.,

$$S|_{\Delta C=0,\omega_0} = \frac{-2\omega_0 C}{\varepsilon_r + 1} \cdot \frac{Z_0}{\prod_{i=1}^{N} \left\{ Z_i^{2\cdot(-1)^{i+N}} \right\}} (N \text{ even}) \tag{23a}$$

$$S|_{\Delta C=0,\omega_0} = \frac{-2\omega_0 C}{\varepsilon_r + 1} \cdot \frac{\prod_{i=1}^{N} \left\{ Z_i^{2\cdot(-1)^{i+N}} \right\}}{Z_0} (N \text{ odd}) \tag{23b}$$

From (23), it follows that the step-impedance CPW structure introduces a multiplicative effect on the overall sensitivity, magnified by the impedance contrast of the different 90° transmission line sections. That is, for sensitivity optimization, it is convenient to set the high/low impedances of the different line sections to as high/low values as possible, as compared to Z_0. Moreover, the 90° line sections must exhibit high characteristic impedance for i odd and low impedance of i even.

C. COMPARISON TO THE EQUIVALENT SENSOR BASED ON A HALF-WAVELENGTH OPEN-ENDED SENSING LINE

As mentioned before, a similar behavior between the proposed OCSRR-based sensor and the fully distributed counterpart (i.e., implemented by means of a 180° open-ended sensing line) is expected. Indeed, according to [2], the sensitivity of such fully distributed sensor (excluding the step-impedance structure) for $\varepsilon_{\text{MUT}} = 1$ is given by

$$\frac{d\phi_\rho}{d\varepsilon_{\text{MUT}}} = \frac{d\phi_\rho}{d\phi_s}\frac{d\phi_s}{d\varepsilon_{\text{MUT}}} = -2\frac{z_0}{Z_s} \cdot \frac{\omega_0 l_s}{2\sqrt{2}c} \frac{1}{\sqrt{\varepsilon_r + 1}} \tag{24}$$

where l_s and Z_s are the length and characteristic impedance, respectively, of the 180° open-ended sensing line, ω_0 is the operating frequency (providing the required 180° electrical length to the uncovered sensing line), and c is the speed of light in vacuum. Taking into account that the phase of the line at Ω_0 can be expressed as

$$\phi_s = \pi = \frac{\omega_0 l_s}{v_p}, \tag{25}$$

where v_p is the phase velocity, given by

$$v_p = \frac{c}{\sqrt{\varepsilon_{\text{eff}}}}, \tag{26}$$

and the effective dielectric constant of a CPW line is

$$\varepsilon_{\text{eff}} = \frac{\varepsilon_r + \varepsilon_{\text{MUT}}}{2}, \tag{27}$$

expression (24) can be written as

$$\frac{d\phi_\rho}{d\varepsilon_{\text{MUT}}} = -\frac{Z_0}{Z_s}\frac{\pi}{\varepsilon_r + 1} \tag{28}$$

Using the equivalence between a 180° open-ended line and a parallel resonant tank with inductance L and capacitance C (see Appendix A), the impedance of the sensing line in (28), Z_s, can be replaced with the elements of the equivalent LC resonator according to expression (A.8) in the Appendix A. With this mapping, the sensitivity given by (28) is identical to the one given by (17). Naturally, if the step-impedance structure is present, the sensitivity of both the OCSRR-based sensor and the sensor implemented by means of a 180° sensing line, are also identical and given by expressions (23).

The identical behavior of both sensor types, predicted by the sensitivity analysis, will be validated in the next section. Nevertheless, it should be mentioned, and highlighted, that such identical sensitivities are obtained for sensor operation at Ω_0 (the intrinsic resonance of the bare OCSRR, which should be identical to the angular frequency providing a 180° sensing line), and in the limit of small perturbations. Moreover, the mapping indicated in (A.8) must be satisfied. Despite the similar achievable performance, the key advantage of the novel OCSRR-based sensors, as compared to the fully distributed counterparts, concerns the size of the sensing region. It is substantially smaller in the OCSRR-based sensor, by virtue of the small electrical size of the OCSRR. This size reduction of the sensing region, and the derivation of design guidelines, given by expressions (17) and (23) for the OCSRR-terminated CPW and for the same structure including the step-impedance configuration, respectively, constitute the main relevant contributions of the present paper (additionally, a method to estimate the loss tangent of the MUT in these reflective-mode phase-variation sensors is reported for the first time, as demonstrated in Section V).

IV. SENSOR VALIDATION

For sensor validation, three different OCSRR-terminated CPW based sensors have been designed and fabricated. In all cases, the considered substrate is the *Rogers RO3010* with

dielectric constant $\varepsilon_r = 10.2$, thickness $h = 1.27$ mm, and loss tangent $\tan\delta = 0.0022$. There is not a specific reason for choosing such substrate, with relatively high dielectric constant. Indeed, reducing the dielectric constant of the substrate helps in increasing the sensitivity, but the actual impact on the sensitivity in the proposed sensors is achieved by the step-impedance discontinuities. The difference between the three sensors concerns the step impedance configuration, being the OCSRR-terminated CPW sensing region identical in all the cases (dimensions indicated in Fig. 2). Thus, in sensor A, the structure merely consists of the sensing part (i.e., the OCSRR-terminated CPW), whereas in sensors designated as B and C, the devices include a step-impedance configuration for sensitivity enhancement. For sensor B, a single high-impedance 90° line section ($N = 1$) cascaded to the OCSRR-terminated CPW is considered, whereas sensor C is implemented by including two high/low impedance 90° line sections ($N = 2$). In sensor B, the characteristic impedance of the high-impedance 90° line section has been set to $Z_1 = 70\ \Omega$. In sensor C, an identical impedance for the high-impedance 90° line adjacent to the sensing region has been considered, whereas the impedance of the cascaded low-impedance 90° line section has been set to $Z_2 = 35.35\ \Omega$.

Additionally, we have designed the fully distributed counterparts of sensors A, B and C, designated as A′, B′ and C′, respectively, where the OCSRR-terminated CPW sensing structure has been replaced with a low-impedance 180° open-ended sensing line. The impedance of such line is calculated according to expression (A.8) of the Appendix A, which gives $Z_s = 35.35\ \Omega$ (the extracted values of L and C are given in the caption of Fig. 3).

The photographs of all these sensors, fabricated by means of the *LPKF H100* drilling machine, are depicted in Fig. 5, where the dimensions are indicated. It should be mentioned that for sensors B and C, the length of the high-impedance 90° line adjacent to the OCSRR has been adjusted (reduced as compared to the nominal value) in order to compensate for the phase shift generated by the parasitic capacitance that appears in the contact plane between such line and the OCSRR. For that purpose, we have forced the simulated phase of the reflection coefficient of sensor B (without access lines) to be 180°, corresponding to a short circuit, since this is the impedance that should be seen from the input port when a 90° line is cascaded to the OCSRR operating at its intrinsic resonance frequency. Obviously, for sensor C, inferred from sensor B by cascading a low-impedance 90° line, the input impedance should correspond to an open-circuit. Nevertheless, this does not need any modification in the length of this added line, since the parasitic capacitance of the step-impedance discontinuity has been found to be negligible. Thus, the length l_1 that appears in the caption of Fig. 5 (in reference to the line section designated with the index $i = 1$) is only valid for sensors B′ and C′. For sensors B and C, such reduced length is $l_1 = 16.15$ mm. Note also that in sensors A, B and C, the ground plane regions of the CPW are short-circuited by means of vias and strips etched

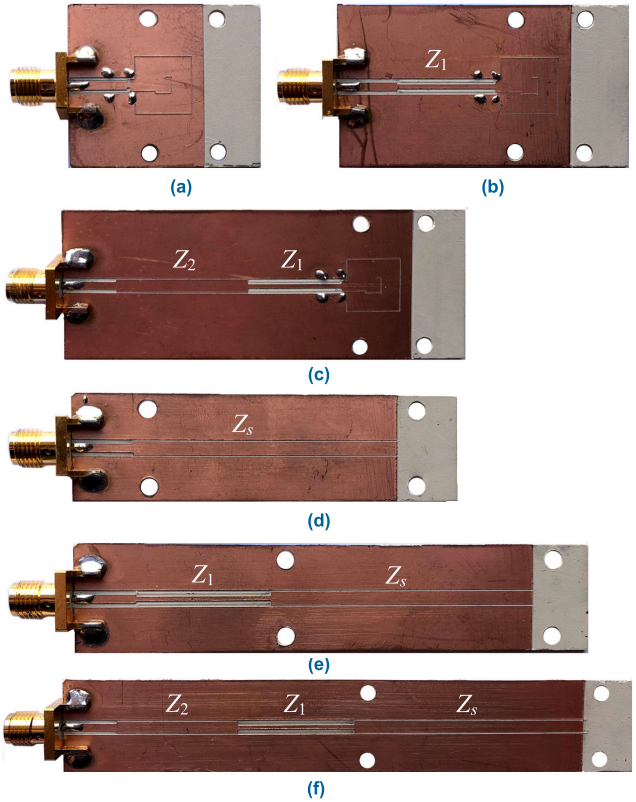

FIGURE 5. Photographs of sensors A (a), B (b), C (c), A′ (d), B′ (e) and C′ (f). The dimensions of the OCSRR-terminated CPW are given in Fig. 2. The dimensions of the high/low step-impedance CPW line sections (in mm) are: $w_1 = 0.72$, $G_1 = 1.04$, $l_1 = 22.40$ (for sensors B′ and C′ only), $w_2 = 2.25$, $G_2 = 0.28$, $l_2 = 22.53$. The dimensions of the low-impedance 180° open-ended sensing line are (in mm): $w_s = 2.25$, $G_s = 0.28$, $l_s = 44.78$. In all the cases, the dimensions of the access line (50 ohm) are (in mm): $w_0 = 1.39$, $G_0 = 0.71$, $l_0 = 10$.

in the back-substrate side, in order to avoid the appearance of the parasitic slot mode (this is necessary since the OCSRRs do not exhibit axial symmetry).

Prior to sensor validation through experiment, we have carried out full-wave simulations by means of the *CST Microwave Studio* commercial software. Specifically, we have considered the sensing regions (OCSRR-terminated CPW in sensors A, B and C, and 180° open-ended line in sensors A′, B′, and C′) covered by a semi-infinite MUT with varying dielectric constant. The simulated phases for all the sensors, as a function of the dielectric constant of the MUT, $\varepsilon_{\mathrm{MUT}}$, are depicted in Fig. 6. It should be mentioned that the frequency of operation has been set to $f_0 = \omega_0/2\pi = 1.442$ GHz, the intrinsic resonance frequency of the bare OCSRR (and the frequency providing an electrical length of 180° to the bare sensing line). By numerically obtaining the derivative of such phases with $\varepsilon_{\mathrm{MUT}}$, the sensitivities are inferred (the results are also included in Fig. 6).

It can be appreciated that the sensitivities in the limit of small perturbations (i.e., for $\Delta C = 0$ pF, or $\varepsilon_{\mathrm{MUT}} = 1$) are nearly identical for the OCSRR-based and the open-ended 180° line-based sensors. The values are indicated in Fig. 6. Moreover, these values coincide

with the theoretical predictions, given by expressions (17) or (23), to a good approximation. Thus, with these simulation results, the sensitivity analysis and the equivalence between the OCSRR-based sensors and the fully distributed counterparts is demonstrated. The multiplicative effect of the step-impedance configuration, first reported in [1], provides a maximum sensitivity for sensors C and C′ of −83.35° and −80.14°, respectively (simulated values). These sensitivities are very high, especially for sensor C, taking into account the small size of the sensing region. A figure of merit (FoM) in phase-variation sensors is the ratio between the sensitivity and the size of the sensing region expressed in terms of the squared guided wavelength, λ^2. The values for sensors C and C′ (for the maximum sensitivity) are FoM = 5643°/λ^2 and FoM = 801°/λ^2, respectively. The value for sensor C is very competitive thanks to the use of an OCSRR as sensing element (and obviously, by virtue of the multiplicative effect of the step-impedance configuration).

Finally, we have experimentally validated the sensors of Fig. 5 by covering the sensing regions with several commercially available (uncladded) microwave substrates, and with a MUT sample (PLA) fabricated with a 3D printer (the *Ultimaker* 3 *Extended*). In all the cases, the thickness of the MUT samples is roughly 3 mm, so that such samples can be considered to be semi-infinite in the vertical direction (stacking of two 1.5-mm thick samples, available in our laboratory, has been carried out for that purpose). The measured phases at the operating frequency for such MUTs, inferred by means of the *Keysight 85072A* vector network analyzer, are also included in Fig. 6. Actually, we have performed the measurements three times, in order to ensure that the measurements are repetitive (the error bars are included in Fig. 6). Nevertheless, the measurements have not been carried out by varying the environmental conditions (temperature and humidity) in a controllable way. The agreement with the simulated data points is good in all the cases, and, consequently, the reported sensors are experimentally validated.

We would like to mention that the analytical study carried out in the previous section and sensor validation by means of electromagnetic simulation and phase measurements consider that the MUT is thick enough to ensure that the electromagnetic field lines do not reach the MUT/air interface. With such semi-infinite MUT approximation, the maximum sensitivity, i.e., the one corresponding to $\varepsilon_{MUT} = 1$, can be predicted by means of simple expressions (17 or 23, depending on the sensor configuration). The simplicity of such expressions is consequence of the compact dependence of the capacitance of the OCSRR on the dielectric constant of the MUT, given by (3) and valid for semi-infinite MUTs, as mentioned before. Nevertheless, it does not mean that the dielectric constant of thin MUT samples cannot be inferred by means of the proposed sensors. Similar curves to those depicted in Fig. 6 can be generated for thinner MUT samples, and from the measured phase, the dielectric constant of the MUT sample can be obtained. Obtaining the OCSRR capacitance as a function of both the dielectric constant and

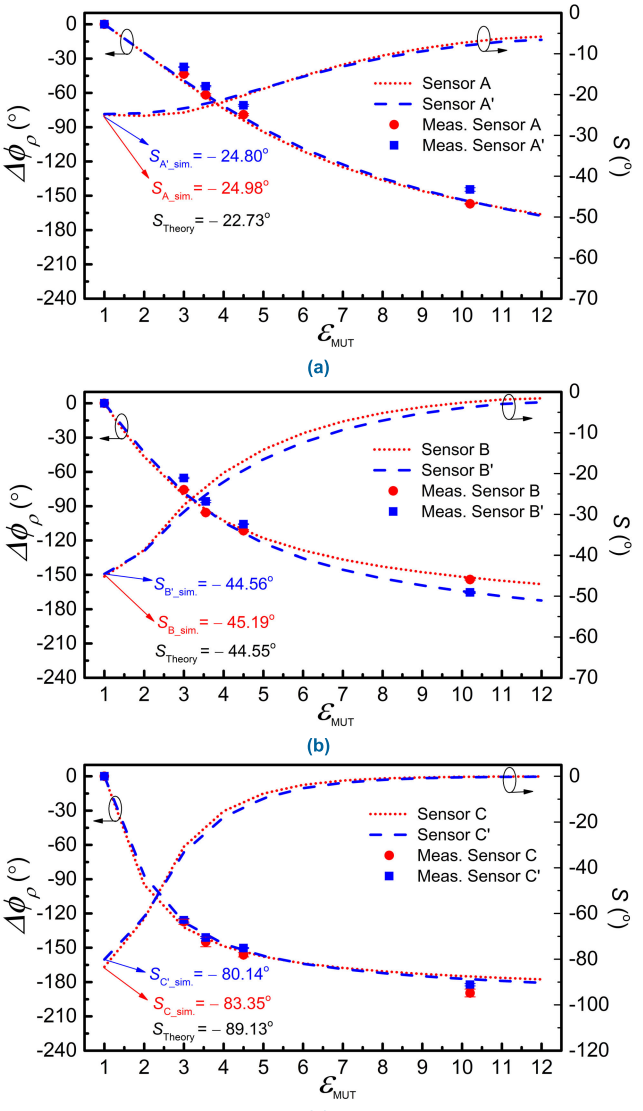

FIGURE 6. Differential phase ($\Delta\phi_\rho = \phi_\rho - \phi_{\rho,\varepsilon MUT=1}$), measured at f_0, and sensitivity for the designed and fabricated sensors. (a) Sensors A and A′; (b) sensors B and B′; (c) sensors C and C′.

thickness of the MUT [i.e., an equivalent expression to (3) for samples with limited thickness] is also possible, but this aspect is out of the scope of this paper.

V. EFFECTS OF LOSSES

In this paper, the main aim is the implementation of highly sensitive sensors devoted to the determination of the dielectric constant of the MUT, or other magnitudes related to it, e.g., material composition, defect detection, etc. Nevertheless, the effects of losses on the sensitivity should be analyzed. For that purpose, we have considered as representative sensor for this study sensor A, based solely on the OCSRR-terminated CPW. The circuit model by including losses is depicted in Fig. 7. Substrate and conductor losses are modelled by the conductance G, whereas G_{MUT} accounts for MUT losses. The input impedance of the structure, evaluated at the operating

frequency, Ω_0, is

$$Z_{\text{in}} = \frac{G_T}{G_T^2 + \omega_0^2 \Delta C^2} + j\omega_0 \left\{ L_s - \frac{\Delta C}{G_T^2 + \omega_0^2 \Delta C^2} \right\} \quad (29)$$

where $G_T = G + G_{\text{MUT}}$. Using (4), with Z_{in} given by (29), the reflection coefficient is obtained, and from it, the phase is found to be

$$\phi_\rho = \arctan \left\{ -\frac{\omega_0 \left(L_s - \frac{\Delta C}{G_T^2 + \omega_0^2 \Delta C^2} \right)}{Z_0 \left(1 - \frac{G_T}{Z_0 (G_T^2 + \omega_0^2 \Delta C^2)} \right)} \right\} + \text{tarctan} \left\{ -\frac{\omega_0 \left(L_S - \frac{\Delta C}{G_T^2 + \omega_0^2 \Delta C^2} \right)}{Z_0 \left(1 + \frac{G_T}{Z_0 (G_T^2 + \omega_0^2 \Delta C^2)} \right)} \right\} \quad (30)$$

Under the assumption that losses are small, we can assume that

$$\frac{G_T}{Z_0 (G_T^2 + \omega_0^2 \Delta C^2)} \ll 1 \quad (31)$$

and from the first-order Taylor expansion $\arctan[A/(1 + x)] = \arctan[A] - Ax/(1 + A^2)$, considering small x values, expression (30) can be approximated by

$$\phi_\rho = 2 \arctan \left\{ -\frac{\omega_0}{Z_0} \left(L_s - \frac{\Delta C}{G_T^2 + \omega_0^2 \Delta C^2} \right) \right\} \quad (32)$$

If we now assume that $\Delta G_T^2 \ll \omega_0^2 C^2$, it follows that (30) is identical to (8), the lossless case, evaluated at $\Omega = \omega_0$. Note that this last condition is necessary in order to satisfy (31) if G_T is small. This is the usual situation with low-loss samples. However, for MUTs with extremely small dielectric constants (i.e., $\varepsilon_{\text{MUT}} \to 1$, or $\Delta C \to 0$), the condition $G_T^2 \ll \omega_0^2 \Delta C^2$ is not necessarily true despite the fact that G_T is small. Let us consider now that $G_T^2 \gg \omega_0^2 \Delta C^2$, with G_T small. In this case, the intrinsic impedance (i.e., excluding the effects of L_s) of the lossy OCSRR is dominated by the resistive part (see 29), which is necessarily high by virtue of the small value of G_T and because $G_T^2 \gg \omega_0^2 \Delta C^2$ (indeed, the real part of the impedance can be approximated by $1/G_T$). Under these conditions, the impedance seen from the input port is essentially an open-circuit, and the phase of the reflection coefficient is null. Such phase is also the resulting one for the lossless case and $\Delta C \to 0$, since the OCSRR opens at the operating frequency.

From the previous analysis, it can be concluded that the effects of losses on the phase of the reflection coefficient and, consequently on the sensitivity, are not significant, provided losses are small (this is the case in the considered sensors and the MUT samples used for experimental validation). Nevertheless, we have inferred the phase of the reflection coefficient of the structure as a function of both the dielectric constant, ε_{MUT}, and the loss tangent, $\tan\delta_{\text{MUT}}$, of the MUT, by full-wave electromagnetic simulation using *CST Microwave Studio*. The considered input dynamic range for the dielectric constant of the MUT is the one of Fig. 6, whereas for the loss tangent, it is limited to the interval [0.001-0.01] (note that the variation in $\tan\delta_{\text{MUT}}$ modifies G_T through G_{MUT}, i.e., G is kept unaltered). The results are depicted in Fig. 8(a), which shows that the effects of losses on the phase are not relevant, as predicted by the theory. Consequently, from the measurement of the phase of the reflection coefficient, the dielectric constant of the MUT can be directly inferred, provided the MUT is a low-loss material. Although the effects of losses on the phase of the reflection coefficient have been analyzed on the basis of sensor A, the same conclusions apply to sensors B and C. Thus, the curves for the different considered sensors shown in Fig. 6 are useful for determining the dielectric constant of the MUT.

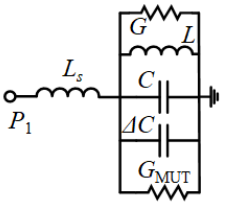

FIGURE 7. Circuit model of the lossy OCSRR-terminated CPW.

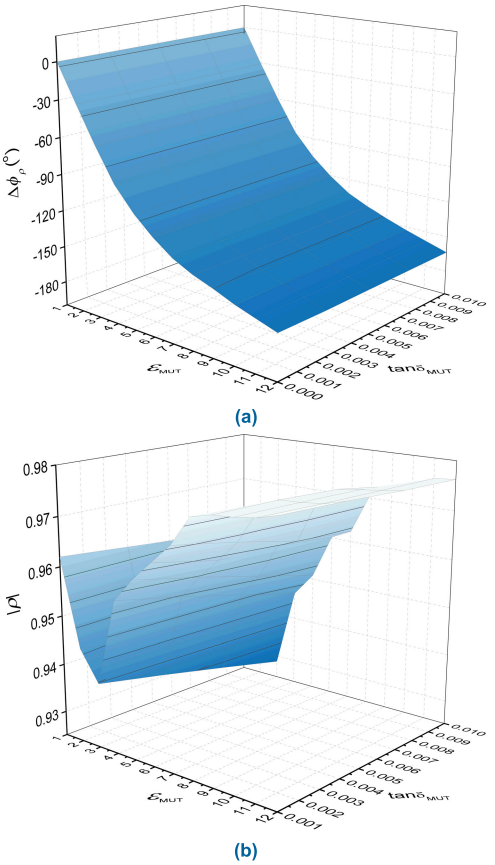

FIGURE 8. Phase (a) and magnitude (b) of the reflection coefficient for sensor A as a function of the dielectric constant and loss tangent of the MUT, inferred from electromagnetic simulation.

Another important aspect to consider is to what extent the proposed sensors are useful for determining the loss tangent of the MUT. In general, resonant methods, based on the measurement of the magnitude of the resonant notch or peak, are convenient for that purpose. For the proposed sensors, a semi-lumped resonator (the OCSRR) subjected to the effects of losses in the MUT (and also in the sensing structure) is the considered sensing element. Losses should be manifested by a reduction in the magnitude of the reflection coefficient at resonance. We have obtained (through full-wave simulation) the magnitude of the reflection coefficient at the resonance frequency of the bare OCSRR, Ω_0, i.e., $|\rho| = |S_{11}|$, as a function of $\varepsilon_{\rm MUT}$ and $\tan\delta_{\rm MUT}$. The results, depicted in Fig. 8(b), show that $|S_{11}|$ does not depend solely on $\tan\delta_{\rm MUT}$, but also on $\varepsilon_{\rm MUT}$. Since $\varepsilon_{\rm MUT}$ can be determined from Fig. 8(a), or from calibrated curves inferred from the experimental data in Fig. 6, the loss tangent of the MUT, $\tan\delta_{\rm MUT}$, can potentially be inferred from the measured value of $|S_{11}|$ and the value of $\varepsilon_{\rm MUT}$. However, this approach needs experimental calibration curves for the dependence of $|\rho|=|S_{11}|$ on $\varepsilon_{\rm MUT}$ and $\tan\delta_{\rm MUT}$, and this is not easy due to the lack of available materials (MUTs) with a wide range of loss tangents.

To solve the previous issue, an analytical approach, based on the lossy circuit model and the link between the loss tangent of the MUT and the model parameters, is proposed next. The key aspect is to determine $G_{\rm MUT}$ from the experimental data relative to the modulus of the reflection coefficient. The modulus of the reflection coefficient at Ω_0 is given by

$$|\rho| = \sqrt{\frac{\omega_0^2\left(L_s - \frac{\Delta C}{G_T^2+\omega_0^2\Delta C^2}\right)^2 + Z_0^2\left(1 - \frac{G_T}{Z_0(G_T^2+\omega_0^2\Delta C^2)}\right)^2}{\omega_0^2\left(L_s - \frac{\Delta C}{G_T^2+\omega_0^2\Delta C^2}\right)^2 + Z_0^2\left(1 + \frac{G_T}{Z_0(G_T^2+\omega_0^2\Delta C^2)}\right)^2}} \tag{33}$$

By considering absence of MUT (i.e., OCSRR surrounded by air), $\Delta C = 0$ and $G_{\rm MUT} = 0$, and the reflection coefficient at Ω_0 simplifies to

$$|\rho|_{\rm air} = \sqrt{\frac{\omega_0^2 L_S^2 + Z_0^2\left(1 - \frac{1}{Z_0 G}\right)^2}{\omega_0^2 L_S^2 + Z_0^2\left(1 + \frac{1}{Z_0 G}\right)^2}} \tag{34}$$

Using (34) and the measured value of $|\rho|_{air}$, the circuit parameter modelling the effects of sensor losses, G, can be isolated. The result is as follows

$$G = \frac{Z_0\left(1+|\rho|_{\rm air}^2\right) \pm \sqrt{4Z_0^2|\rho|_{\rm air}^2 - \omega_0^2 L_S^2\left(1-|\rho|_{\rm air}^2\right)^2}}{\left(\omega_0^2 L_S^2 + Z_0^2\right)\left(1-|\rho|_{\rm air}^2\right)} \tag{35}$$

where the negative sign must be taken, as justified in Appendix B. The measured magnitude of the reflection coefficient at resonance for the Sensor A when the OCSRR is surrounded by air is $|\rho|_{\rm air} = 0.923$, and the corresponding conductance is found to be $G = 8.01 \times 10^{-4}$ S.

The next step is to load the OCSRR with the MUT and measure the modulus of the reflection coefficient at Ω_0, $|\rho|$. Using (33), G_T can be numerically calculated, provided the reactive parameters of the OCSRR, as well as ΔC, are known (note that isolating G_T in expression 33 represents an excessive analytical burden). Therefore, the conductance associated to the MUT sample can be simply obtained as $G_{\rm MUT} = G_T - G$, since G is calculated from the previous step.

In the previous approach, the measured modulus of the reflection coefficient at Ω_0 is the variable considered for determining G and G_T. At such frequency, the intrinsic impedance of the OCSRR (excluding the effect of L_s) is not purely resistive except for $\varepsilon_{\rm MUT} = 1$ (or $\Delta C = 0$). Thus, the modulus of the reflection coefficient experiences a significant variation with frequency at that frequency, and the accuracy of the method is very limited, especially taking into account that the samples under consideration may exhibit loss tangents comparable to the one of the considered sensor substrates. Thus, we have proceeded by recording the measured modulus of the reflection coefficient at the resonance frequency of the OCSRR covered by each MUT sample. This frequency can be easily identified from the measured data, since at resonance, the magnitude of the reflection coefficient is a minimum. Using an expression identical to (35), the total conductance for each sample, G_T, can be obtained. For that purpose, $|\rho_{\rm air}|$ and Ω_0 must be replaced with $|\rho_{\rm MUT}|$ and $\Omega_{0,\rm MUT}$, respectively, in (35), where $\Omega_{0,\rm MUT}$ is the intrinsic resonance frequency of the OCSRR loaded with the MUT, and $|\rho_{\rm MUT}|$ is the measured modulus of the reflection coefficient at that frequency. From the different values of G_T, corresponding to the MUT samples used in the previous experimental validation, the conductance of each sample, $G_{\rm MUT}$, has been inferred (it is shown in the third column of Table 1). As mentioned before, the experimental reflection coefficients are those corresponding to Sensor A.

The loss tangent and the conductance of the MUT are related by [10]

$$\tan\delta_{\rm MUT} = \frac{G_{\rm MUT}}{\omega_0 C_{\rm MUT}} \tag{36}$$

where $C_{\rm MUT}$ is the portion of the total capacitance of the OCSRR ($C' = C + \Delta C$) corresponding to the MUT (see Fig. 9). Note that, according to this figure, the capacitance of the uncovered OCSRR can be expressed as $C = C_{\rm subs} + C_{\rm air}$, whereas the capacitance of the loaded OCSRR is $C' = C + \Delta C = C_{\rm subs} + C_{\rm MUT}$, where $C_{\rm subs}$ and $C_{\rm air}$ are the capacitances of the substrate region and air (uncovered OCSRR), respectively, see Fig. 9. Thus, the capacitance of the MUT can be expressed as

$$C_{\rm MUT} = C' - C_{\rm subs} = C\frac{\varepsilon_{\rm MUT}}{1+\varepsilon_{\rm MUT}} \tag{37}$$

TABLE 1. Loss tangent and relevant parameters for the different considered MUT samples.

MUT	$\lvert\rho_{MUT}\rvert$	G_{MUT} ×10^{-4} (S)	ε_{MUT}	tan $\delta_{MUT,ex}$	tan $\delta_{MUT,th}$
PLA	0.915	0.87	3	0.0073	0.008
RO4003C	0.915	0.87	3.55	0.0062	0.0021
FR4	0.889	3.75	4.5	0.0210	0.02
RO3010	0.901	2.41	10.2	0.0060	0.0022

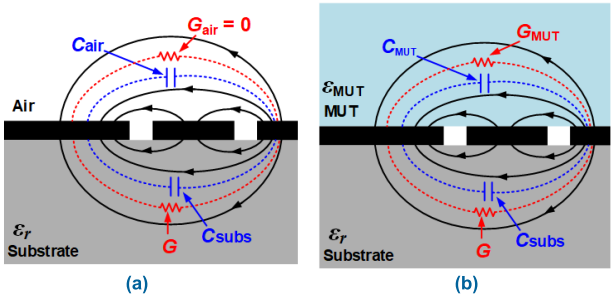

FIGURE 9. Cross-sectional view of the slot region of the OCSRR, with electric field lines and contributions to the total OCSRR capacitance and dielectric conductance. (a) Uncovered OCSRR; (b) MUT-covered OCSRR.

where (3) and

$$C_{\text{subs}} = C' \frac{\varepsilon_r}{\varepsilon_{\text{MUT}} + \varepsilon_r} \tag{38}$$

have been used. It should be mentioned that the validity of (38) requires not only a semi-infinite MUT in the vertical direction, but also a semi-infinite substrate. This approximation is adopted in this work, provided the considered substrate is relatively thick (and the slots of the OCSRR are very narrow). Introducing (37) in (36), the loss tangent of the MUT, in terms of well-known parameters (ε_r and Ω_0) or previously calculated variables (C, G_{MUT}, and ε_{MUT}), can be obtained, i.e.,

$$\tan\delta_{\text{MUT}} = \frac{G_{\text{MUT}}(\varepsilon_r + 1)}{C\omega_0\varepsilon_{\text{MUT}}} \tag{39}$$

Using (39), the loss tangent of the different samples has been estimated. The obtained values (tan $\delta_{MUT,ex}$) are depicted in Table 1, where they are compared with the theoretical values reported in the datasheets, and designated as tan $\delta_{MUT,th}$ (for the PLA MUT sample, fabricated by means of a 3D printer, $\delta_{MUT,th}$ has been alternatively obtained by means of a resonant cavity).

According to Table 1, the method reasonably predicts the value of the loss tangent of the considered materials, although the discrepancy is higher for the MUTs exhibiting a smaller loss factor. Nevertheless, it should be taken into account the considered approximations, the effects of connectors, and the difficulty to accurately measure the magnitude of the reflection coefficient. The proposed sensors are especially suited for the accurate and highly sensitive determination of the real part of the permittivity, from the measurement of the phase of the reflection coefficient at a single frequency. Nevertheless, this section demonstrates that the sensors can be used to estimate the loss factor of the considered MUT samples (in liquids, with higher loss tangents, or other lossy materials, it is expected that the sensors provide also a reasonable estimation of the loss factor).

TABLE 2. Comparison of various phase variation-sensors.

Ref.	Mode	Size* (λ^2)	Max. Sensitivity	FoM (°/λ^2)
[1]	REFLECTIVE	0.025	528.7°	21148
[2]	REFLECTIVE	0.100	45.5°	455
[30]	TRANSMISSION	---	600 dB	---
[32]	TRANSMISSION	---	54.8°	---
[38]	TRANSMISSION	12.90	415.6°	32.2
[40]	TRANSMISSION	0.075	25.3 dB	---
[41]	TRANSMISSION	0.020	17.6 dB	---
[56]	TRANSMISSION	0.030	7.7°	257
[57]	TRANSMISSION	0.040	20.0°	500
Sens. C'	REFLECTIVE	0.100	80.14°	801
Sens. C	REFLECTIVE	0.015	83.35°	5643

*The size corresponds to the sensing region, not to the whole sensing structure.

VI. COMPARISON WITH OTHER PHASE VARIATION SENSORS

Table 2 includes a list of various phase-variation sensors recently reported, and their main relevant parameters, as well as other characteristics of interest. The table is restricted to phase-variation sensors, since comparing sensors with different sensing principle is difficult (and even meaningless).

In view of the table, the proposed sensor C exhibits an excellent FoM, by virtue of the small area of the sensing region. Note that the FoM is by far superior to the one of the equivalent sensors implemented by means of a 180° open-ended sensing line (sensor C'). The sensitivity in the reflective-mode sensor reported in [1] is very huge, and for this reason the FoM is very high, despite the fact that the size of the sensing region is not as small as the one of the OCSRR-based sensors presented in this paper. Nevertheless, it should be noted that further increasing the sensitivity in the proposed sensors and sensor [1] (and [2]) is possible by merely cascading additional quarter-wavelength high/low impedance transmission line sections. It should be mentioned that sensors C and C′ in this paper, as well as the optimum sensor presented in [1], include two ($N = 2$) high/low impedance 90° line sections (plus the sensing line or OCSRR). However, the sensors presented in this paper are implemented in CPW technology, whereas the sensors in [1] were fabricated in microstrip technology in a different substrate (with the possibility of implementing 90° line sections with a larger impedance contrast).

Line meandering, as reported in the device presented in [38], is a technique to enhance the sensitivity, avoiding the implementation of sensing regions with excessively elongated shape factors. However, the resulting FoM in these sensors is not very good. Also, phase-variation sensors based on slow-wave transmission lines have been reported [56], [57]. In such sensors, the sensitivity is improved, as compared to that of ordinary meandered lines with similar sensing area.

However, the reported sensitivities and FoM are not as competitive as those of the sensors reported in the present paper.

We would like to mention that other phase-variation sensors based on electro-inductive wave (EIW) [40] and composite right/left-handed (CRLH) [30] artificial lines have been reported, but in such sensors the phase information was converted to magnitude information. Nevertheless, these sensors are also included in the comparative Table 2. Though these sensors are competitive in terms of sensitivity and size, their main limitation is the lack of robustness due to potential effects of detuning (this is particularly critical in the narrowband structures based on EIW transmission lines). By contrast, the proposed sensors are based on a single resonant element, and sensor design and fabrication are relatively simple. In the sensors reported in [41], based on meandered sensing lines and operating in differential mode, the phase information is also transformed to magnitude information. The sensitivity in these sensors is reasonably good, and sensor design is simple, but the total sensor size is large since two rat-race couplers are used for phase-to-magnitude transformation.

In summary the combination of size (sensing region), sensitivity, simplicity of design/fabrication, and device operation (single-frequency and reflective mode), makes the proposed sensors strong candidates for applications in several scenarios, including dielectric characterization of solids and defect detection. By adding a fluidic channel on top of the OCSRR, or by submersing the sensitive part of the structure in a certain MUT liquid, these sensors can also be useful for the characterization of liquid samples. Specifically, sensing in industrial processes (e.g., wine fermentation analysis), and bio-sensing (e.g., electrolyte content in blood or urine), among others, are envisaged as potential applications.

VII. CONCLUSION

In conclusion, highly-sensitive one-port reflective-mode phase-variation sensors useful for dielectric characterization of solid samples have been presented in this paper. The sensing element is an electrically small planar resonator, the OCSRR, which is connected as a termination load of a step-impedance CPW transmission line. It is demonstrated in this paper that the step-impedance transmission line is useful to boost up the sensitivity. The sensitivity achieved in one of the proposed sensors (sensor C) is as high as $-83.35°$, considering as output variable the phase of the reflection coefficient, and the dielectric constant of the MUT sample as input variable. However, the main relevant aspect of the proposed sensor is the small size of the sensing region. Consequently, the main figure of merit of these sensors, the ratio between the (maximum) sensitivity and the surface of the sensing region expressed in terms of the squared wavelength, is very competitive (particularly, the figure of merit has been found to be FoM $= 5643°/\lambda^2$ in the designed OCSRR-based sensor exhibiting the highest sensitivity, i.e., sensor C). It has also been demonstrated in the paper that the effects of both MUT and sensor losses do not affect the dependence of the phase of the reflection coefficient (the output variable) with the dielectric constant of the MUT, provided losses are small. Moreover, an analytical method to estimate the loss tangent of the MUT from the measurement of the magnitude of the reflection coefficient at the resonance frequency of the MUT-loaded OCSRR, has been reported and experimentally validated. Besides the small size of the sensing region, the planar nature and one-port configuration of the whole sensing structure, as well as the operation at a single frequency, are other important aspects of the proposed device. Though in this paper the main focus has been the dielectric characterization of solid samples, these sensors may also be interesting for the study and characterization of liquid samples (dielectric characterization, composition, determination of solute content in mixtures, etc.). For such purpose, a fluidic channel may be added on top of the sensing region. Alternatively, by virtue of the reflective-mode one-port operation, submersible sensors based on the proposed OCSRR-based structures can be also envisaged (these aspects are left for a future work).

APPENDIX A
EQUIVALENCE BETWEEN A 180° OPEN-ENDED SENSING LINE AND A PARALLEL LC SENSING RESONATOR

The reactance of an open-ended line with impedance Z_s and phase ϕ_s, at certain frequency Ω_0, perturbed by the presence of a MUT on top of it, and neglecting losses, can be expressed as [55]

$$\chi_{\text{in,line}} = -(Z_s + \Delta Z_s)\cot(\phi_s + \Delta\phi_s) \tag{A.1}$$

where ΔZ_s and $\Delta\phi_s$ are the variations experienced by the impedance and the phase of the line, respectively, due to the MUT. For $\phi_s = \pi$, the case under study, and small perturbations, (A.1) can be approximated by

$$\chi_{\text{in,line}} = -\frac{Z_s}{\Delta\phi_s} \tag{A.2}$$

On the other hand, the reactance of a parallel LC resonator describing a certain planar resonant particle (e.g., an OCSRR) perturbed by a MUT is given by (7), excluding L_s, where ΔC accounts for the variation in C caused by the MUT. At the intrinsic resonance frequency of the bare OCSRR, Ω_0, the reactance is

$$\chi_{\text{in}} = -\omega_0 L\frac{C}{\Delta C} \tag{A.3}$$

For small perturbations, $\Delta\phi_s$ can be expressed as

$$\Delta\phi_s = \omega_0\left(\sqrt{L_l(C_l + \Delta C_l)} - \sqrt{L_l C_l}\right) \tag{A.4}$$

where L_l and C_l are the line inductance and capacitance, respectively, corresponding to the considered line section (of electrical length π), and ΔC_l is the variation of the line capacitance caused by the MUT. Since for small perturbations ΔC_l is necessarily small, (A.4) can be expressed as

$$\Delta\phi_s = \omega_0\sqrt{L_l C_l}\left(\sqrt{1 + \frac{\Delta C_l}{C_l}} - 1\right) \tag{A.5}$$

$$\frac{\frac{dN}{d|\rho|^2_{air}}}{\frac{dD}{d|\rho|^2_{air}}} = \frac{Z_0 - \frac{1}{2}\left(4Z_0^2|\rho|^2_{air} - \omega_0^2 L_s^2\left(1-|\rho|^2_{air}\right)^2\right)^{-\frac{1}{2}}\left(4Z_0^2 + 2\omega_0^2 L_s^2\left(1-|\rho|^2_{air}\right)\right)}{-(^2_0 L_s^2 + Z_0^2)} \tag{B.1}$$

which in turn can be written as

$$\Delta\phi_s = \omega_0\sqrt{L_l \Delta C_l}\left(\frac{C_l}{2C_l}\right) \tag{A.6}$$

or

$$\Delta\phi_s = \pi\frac{\Delta C_l}{2C_l} \tag{A.7}$$

By equating (A.2) and (A.3), using (A.7) and identifying $\Delta C_l/C_l$ with $\Delta C/C$, it follows that:

$$Z_s = \frac{\pi L\omega_0}{2} = \frac{\pi}{2}\sqrt{\frac{L}{C}} \tag{A.8}$$

Thus, in order to obtain identical responses for small perturbations in the sensor based on a parallel LC resonator and the one based on an open-ended 180° sensing line, L and C must satisfy

$$L = \frac{2Z_s}{\pi\omega_0}, \quad C = \frac{\pi}{2Z_s\omega_0} \tag{A.9}$$

and the equivalence between ΔC and $\Delta\phi_s$ is given by:

$$\Delta\phi_s = \pi\frac{\Delta C}{2C} \tag{A.10}$$

Indeed, the relative variation in the line capacitance of a CPW, $\Delta C_l/C_l$, caused by a certain semi-infinite MUT, is identical to the relative variation in the capacitance of an OCSRR, $\Delta C/C$, that results when it is covered with an identical MUT. This means that using (A.8), or (A.9), suffices to obtain identical sensitivities in the limit of small perturbations in both considered sensors, as it is demonstrated in Section IV. However, if the purely distributed sensor is implemented, e.g., in microstrip technology, in such case $\Delta C_l/C_l = \Delta C/C$ for different dielectric constants of the MUT. Nevertheless, we can express the differential phase as $d\phi_s = \pi \cdot dC'/2C$, and thereby

$$\frac{d\phi_\rho}{d\Delta C} = \frac{d\phi_\rho}{dC'} = \frac{\pi}{2C}\cdot\frac{d\phi_\rho}{d\phi_s} \tag{A.11}$$

where the derivative in the right-hand side member is (see 24)

$$\frac{d\phi_\rho}{d\phi_s} = -\frac{2Z_0}{Z_s} \tag{A.12}$$

Introducing Z_s as given by (A.8) in (A.12), and the result in (A.11), one obtains

$$\frac{d\phi_\rho}{d\Delta C} = -2Z_0\omega_0 \tag{A.13}$$

i.e., an expression identical to (15). This further validates the equivalence between the 180° open-ended CPW and the OCSRR sensing structures, with identical sensitivities at small perturbations (provided the mapping A.8 is applied). Note that, for the OCSRR-based sensor, the effect of L_s on the sensitivity for sensor operation at Ω_0 and small perturbations is null.

For 180° microstrip sensing lines, with different dependence of the capacitance of the line with $\varepsilon_{\mathrm{MUT}}$, the sensitivity cannot be identical to the one of the OCSRR-based structure, simply because $\Delta C_l/C_l$ cannot be directly identified with $\Delta C/C$ for a certain value of $\varepsilon_{\mathrm{MUT}}$. However, the sensitivity of the phase of the reflection coefficient with the phase of the line, $d\phi_\rho/d\phi_s$, in any considered line technology, is related to the sensitivity of the reflection coefficient with the capacitance of the resonator in the OCSRR-based sensor, $d\phi_\rho/d\Delta C$, through (A.11), provided $\Delta C_l/C_l$ is identified with $\Delta C/C$.

APPENDIX B
DEPENDENCE OF G ON $|\rho|_{\mathrm{air}}$

Let us consider the circuit model in Fig. 7 with $G_{\mathrm{MUT}} = 0$, corresponding to the bare (uncovered) sensor. According to this model, two extreme cases provide $|\rho|_{air} = 1$, (i) $G = 0$, and (ii) $G = \infty$. For $G = 0$, the impedance seen from the input port is purely reactive and, therefore, $|\rho|_{air} = 1$ regardless of the operating frequency. Moreover, $\rho_{\mathrm{air}} = 1$ at Ω_0, since the LC resonant tank opens at this frequency. For $G = \infty$, the input impedance is merely the one of the inductance L_s, and $|\rho|_{\mathrm{air}} = 1$, as well. In view of (35), it is obvious that considering the positive sign in the numerator and $|\rho|_{\mathrm{air}} = 1$ gives $G = \infty$. However, this case is meaningless from a physical viewpoint since the considered losses are small, and thereby G should be very small. This suggests that the negative sign in (35) is the one to be considered, However, with such sign and $|\rho|_{\mathrm{air}} = 1$, both the numerator and the denominator in (35) vanish. Consequently, in order to obtain the value of G in this case, it is necessary to solve the indeterminacy by applying the L'Hô pital rule. For that purpose, the derivative of both the numerator, N, and the denominator, D, of G with $|\rho|^2_{\mathrm{air}}$ is obtained, and the ratio is found to be (B.1), as shown at the top of the page.

It is apparent from (B.1) that the numerator nulls for $|\rho|^2_{\mathrm{air}} = 1$ (or $|\rho|_{\mathrm{air}} = 1$). Thus, $G = 0$ if $|\rho|_{\mathrm{air}} = 1$ and the negative sign in the numerator of (35) is adopted. Thus, in summary, the conductance G must be obtained from the measured value of $|\rho|_{\mathrm{air}}$, by means of (35), using the negative sign in the numerator.

REFERENCES

[1] J. Munoz-Enano, P. Velez, L. Su, M. Gil, P. Casacuberta, and F. Martin, "On the sensitivity of reflective-mode phase-variation sensors based on open-ended stepped-impedance transmission lines: Theoretical analysis and experimental validation," *IEEE Trans. Microw. Theory Techn.*, vol. 69, no. 1, pp. 308–324, Jan. 2021, doi: 10.1109/TMTT.2020.3023728.

[2] L. Su, J. Munoz-Enano, P. Velez, P. Casacuberta, M. Gil, and F. Martin, "Highly sensitive phase variation sensors based on step-impedance coplanar waveguide (CPW) transmission lines," *IEEE Sensors J.*, vol. 21, no. 3, pp. 2864–2872, Feb. 2021, doi: 10.1109/JSEN.2020.3023848.

[3] M. Puentes, C. Weiss, M. Schussler, and R. Jakoby, "Sensor array based on split ring resonators for analysis of organic tissues," in *IEEE MTT-S Int. Microw. Symp. Dig.*, Baltimore, MD, USA, Jun. 2011, pp. 1–4, doi: 10.1109/MWSYM.2011.5972633.

[4] A. Ebrahimi, W. Withayachumnankul, S. Al-Sarawi, and D. Abbott, "High-sensitivity metamaterial-inspired sensor for microfluidic dielectric characterization," *IEEE Sensors J.*, vol. 14, no. 5, pp. 1345–1351, May 2014.

[5] M. Schueler, C. Mandel, M. Puentes, and R. Jakoby, "Metamaterial inspired microwave sensors," *IEEE Microw. Mag.*, vol. 13, no. 2, pp. 57–68, Mar. 2012.

[6] M. S. Boybay and O. M. Ramahi, "Material characterization using complementary split-ring resonators," *IEEE Trans. Instrum. Meas.*, vol. 61, no. 11, pp. 3039–3046, Nov. 2012.

[7] C.-S. Lee and C.-L. Yang, "Complementary split-ring resonators for measuring dielectric constants and loss tangents," *IEEE Microw. Wireless Compon. Lett.*, vol. 24, no. 8, pp. 563–565, Aug. 2014.

[8] C.-L. Yang, C.-S. Lee, K.-W. Chen, and K.-Z. Chen, "Noncontact measurement of complex permittivity and thickness by using planar resonators," *IEEE Trans. Microw. Theory Techn.*, vol. 64, no. 1, pp. 247–257, Jan. 2016.

[9] L. Su, J. Mata-Contreras, P. Velez, and F. Martin, "Estimation of the complex permittivity of liquids by means of complementary split ring resonator (CSRR) loaded transmission lines," in *IEEE MTT-S Int. Microw. Symp. Dig.*, Pavia, Italy, Sep. 2017, pp. 1–3, doi: 10.1109/IMWS-AMP.2017.8247398.

[10] L. Su, J. Mata-Contreras, P. Vélez, A. Fernández-Prieto, and F. Martín, "Analytical method to estimate the complex permittivity of oil samples," *Sensors*, vol. 18, no. 4, p. 984, Mar. 2018.

[11] A. K. Jha, N. Delmonte, A. Lamecki, M. Mrozowski, and M. Bozzi, "Design of microwave-based angular displacement sensor," *IEEE Microw. Wireless Compon. Lett.*, vol. 29, no. 4, pp. 306–308, Apr. 2019.

[12] A. K. Horestani, J. Naqui, Z. Shaterian, D. Abbott, C. Fumeaux, and F. Martín, "Two-dimensional alignment and displacement sensor based on movable broadside-coupled split ring resonators," *Sens. Actuators A, Phys.*, vol. 210, pp. 18–24, Apr. 2014.

[13] J. Naqui, C. Damm, A. Wiens, R. Jakoby, L. Su, and F. Martin, "Transmission lines loaded with pairs of magnetically coupled stepped impedance resonators (SIRs): Modeling and application to microwave sensors," in *IEEE MTT-S Int. Microw. Symp. Dig.*, Tampa, FL, USA, Jun. 2014, pp. 1–4, doi: 10.1109/MWSYM.2014.6848494.

[14] L. Su, J. Naqui, J. Mata-Contreras, and F. Martin, "Modeling metamaterial transmission lines loaded with pairs of coupled split-ring resonators," *IEEE Antennas Wireless Propag. Lett.*, vol. 14, pp. 68–71, 2015.

[15] L. Su, J. Naqui, J. Mata-Contreras, and F. Martin, "Modeling and applications of metamaterial transmission lines loaded with pairs of coupled complementary split-ring resonators (CSRRs)," *IEEE Antennas Wireless Propag. Lett.*, vol. 15, pp. 154–157, 2016.

[16] J. Naqui, C. Damm, A. Wiens, R. Jakoby, L. Su, J. Mata-Contreras, and F. Martin, "Transmission lines loaded with pairs of stepped impedance resonators: Modeling and application to differential permittivity measurements," *IEEE Trans. Microw. Theory Techn.*, vol. 64, no. 11, pp. 3864–3877, Nov. 2016.

[17] L. Su, J. Mata-Contreras, P. Velez, and F. Martin, "Splitter/combiner microstrip sections loaded with pairs of complementary split ring resonators (CSRRs): Modeling and optimization for differential sensing applications," *IEEE Trans. Microw. Theory Techn.*, vol. 64, no. 12, pp. 4362–4370, Dec. 2016.

[18] P. Vélez, L. Su, K. Grenier, J. Mata-Contreras, D. Dubuc, and F. Martín, "Microwave microfluidic sensor based on a microstrip splitter/combiner configuration and split ring resonators (SRR) for dielectric characterization of liquids," *IEEE Sensors J.*, vol. 17, no. 20, pp. 6589–6598, Oct. 2017.

[19] J. Naqui, M. Durán-Sindreu, and F. Martín, "Novel sensors based on the symmetry properties of split ring resonators (SRRs)," *Sensors*, vol. 11, no. 8, pp. 7545–7553, Jul. 2011.

[20] J. Naqui, M. Durán-Sindreu, and F. Martín, "Alignment and position sensors based on split ring resonators," *Sensors*, vol. 12, no. 9, pp. 11790–11797, Aug. 2012.

[21] A. K. Horestani, C. Fumeaux, S. F. Al-Sarawi, and D. Abbott, "Displacement sensor based on diamond-shaped tapered split ring resonator," *IEEE Sensors J.*, vol. 13, no. 4, pp. 1153–1160, Apr. 2013.

[22] A. K. Horestani, D. Abbott, and C. Fumeaux, "Rotation sensor based on horn-shaped split ring resonator," *IEEE Sensors J.*, vol. 13, no. 8, pp. 3014–3015, Aug. 2013.

[23] J. Naqui and F. Martin, "Transmission lines loaded with bisymmetric resonators and their application to angular displacement and velocity sensors," *IEEE Trans. Microw. Theory Techn.*, vol. 61, no. 12, pp. 4700–4713, Dec. 2013.

[24] J. Naqui and F. Martin, "Angular displacement and velocity sensors based on electric-LC (ELC) loaded microstrip lines," *IEEE Sensors J.*, vol. 14, no. 4, pp. 939–940, Apr. 2014.

[25] A. K. Horestani, J. Naqui, D. Abbott, C. Fumeaux, and F. Martín, "Two-dimensional displacement and alignment sensor based on reflection coefficients of open microstrip lines loaded with split ring resonators," *Electron. Lett.*, vol. 50, no. 8, pp. 620–622, Apr. 2014.

[26] A. Ebrahimi, W. Withayachumnankul, S. F. Al-Sarawi, and D. Abbott, "Metamaterial-inspired rotation sensor with wide dynamic range," *IEEE Sensors J.*, vol. 14, no. 8, pp. 2609–2614, Aug. 2014.

[27] J. Naqui, J. Coromina, A. Karami-Horestani, C. Fumeaux, and F. Martín, "Angular displacement and velocity sensors based on coplanar waveguides (CPWs) loaded with S-shaped split ring resonators (S-SRR)," *Sensors*, vol. 15, no. 5, pp. 9628–9650, Apr. 2015.

[28] J. Mata-Contreras, C. Herrojo, and F. Martin, "Application of split ring resonator (SRR) loaded transmission lines to the design of angular displacement and velocity sensors for space applications," *IEEE Trans. Microw. Theory Techn.*, vol. 65, no. 11, pp. 4450–4460, Nov. 2017.

[29] J. Mata-Contreras, C. Herrojo, and F. Martin, "Detecting the rotation direction in contactless angular velocity sensors implemented with rotors loaded with multiple chains of resonators," *IEEE Sensors J.*, vol. 18, no. 17, pp. 7055–7065, Sep. 2018.

[30] C. Damm, M. Schussler, M. Puentes, H. Maune, M. Maasch, and R. Jakoby, "Artificial transmission lines for high sensitive microwave sensors," in *Proc. IEEE Sensors*, Oct. 2009, pp. 755–758, doi: 10.1109/ICSENS.2009.5398538.

[31] P. Vélez, J. Mata-Contreras, L. Su, D. Dubuc, K. Grenier, and F. Martín, "Modeling and analysis of pairs of open complementary split ring resonators (OCSRRs) for differential permittivity sensing," in *IEEE MTT-S Int. Microw. Symp. Dig.*, Pavia, Italy, Sep. 2017, pp. 1–3, doi: 10.1109/IMWS-AMP.2017.8247338.

[32] F. Ferrández-Pastor, J. García-Chamizo, and M. Nieto-Hidalgo, "Electromagnetic differential measuring method: Application in microstrip sensors developing," *Sensors*, vol. 17, no. 7, p. 1650, Jul. 2017.

[33] P. Velez, K. Grenier, J. Mata-Contreras, D. Dubuc, and F. Martin, "Highly-sensitive microwave sensors based on open complementary split ring resonators (OCSRRs) for dielectric characterization and solute concentration measurement in liquids," *IEEE Access*, vol. 6, pp. 48324–48338, Aug. 2018.

[34] A. Ebrahimi, J. Scott, and K. Ghorbani, "Transmission lines terminated with LC resonators for differential permittivity sensing," *IEEE Microw. Wireless Compon. Lett.*, vol. 28, no. 12, pp. 1149–1151, Dec. 2018.

[35] A. Ebrahimi, J. Scott, and K. Ghorbani, "Differential sensors using microstrip lines loaded with two split-ring resonators," *IEEE Sensors J.*, vol. 18, no. 14, pp. 5786–5793, Jul. 2018.

[36] P. Vélez, J. Muñoz-Enano, K. Grenier, J. Mata-Contreras, D. Dubuc, and F. Martín, "Split ring resonator-based microwave fluidic sensors for electrolyte concentration measurements," *IEEE Sensors J.*, vol. 19, no. 7, pp. 2562–2569, Apr. 2019.

[37] P. Vélez, J. Muñoz-Enano, M. Gil, J. Mata-Contreras, and F. Martín, "Differential microfluidic sensors based on dumbbell-shaped defect ground structures in microstrip technology: Analysis, optimization, and applications," *Sensors*, vol. 19, no. 14, p. 3189, Jul. 2019.

[38] J. Munoz-Enano, P. Velez, M. G. Barba, and F. Martin, "An analytical method to implement high-sensitivity transmission line differential sensors for dielectric constant measurements," *IEEE Sensors J.*, vol. 20, no. 1, pp. 178–184, Jan. 2020.

[39] P. Velez, J. Munoz-Enano, and F. Martin, "Differential sensing based on quasi-microstrip mode to slot-mode conversion," *IEEE Microw. Wireless Compon. Lett.*, vol. 29, no. 10, pp. 690–692, Oct. 2019.

[40] M. Gil, P. Velez, F. Aznar-Ballesta, J. Munoz-Enano, and F. Martin, "Differential sensor based on electroinductive wave transmission lines for dielectric constant measurements and defect detection," *IEEE Trans. Antennas Propag.*, vol. 68, no. 3, pp. 1876–1886, Mar. 2020.

[41] J. Munoz-Enano, P. Velez, M. Gil Barba, J. Mata-Contreras, and F. Martin, "Differential-mode to common-mode conversion detector based on rat-race hybrid couplers: Analysis and application to differential sensors and comparators," *IEEE Trans. Microw. Theory Techn.*, vol. 68, no. 4, pp. 1312–1325, Apr. 2020.
[42] G. Galindo-Romera, F. Javier Herraiz-Martinez, M. Gil, J. J. Martinez-Martinez, and D. Segovia-Vargas, "Submersible printed split-ring resonator-based sensor for thin-film detection and permittivity characterization," *IEEE Sensors J.*, vol. 16, no. 10, pp. 3587–3596, May 2016.
[43] P. Wei, B. Morey, T. Dyson, N. Mcmahon, Y.-Y. Hsu, S. Gazman, L. Klinker, B. Ives, K. Dowling, and C. Rafferty, "A conformal sensor for wireless sweat level monitoring," in *Proc. IEEE Sensors*, Baltimore, MD, USA, Nov. 2013, pp. 1–4, doi: 10.1109/ICSENS.2013.6688376.
[44] L. Su, X. Huang, W. Guo, and H. Wu, "A flexible microwave sensor based on complementary spiral resonator for material dielectric characterization," *IEEE Sensors J.*, vol. 20, no. 4, pp. 1893–1903, Feb. 2020.
[45] M. M. Rodgers, V. M. Pai, and R. S. Conroy, "Recent advances in wearable sensors for health monitoring," *IEEE Sensors J.*, vol. 15, no. 6, pp. 3119–3126, Jun. 2015.
[46] K. Grenier, D. Dubuc, P.-E. Poleni, M. Kumemura, H. Toshiyoshi, T. Fujii, and H. Fujita, "Integrated broadband microwave and microfluidic sensor dedicated to bioengineering," *IEEE Trans. Microw. Theory Techn.*, vol. 57, no. 12, pp. 3246–3253, Dec. 2009.
[47] T. Chretiennot, D. Dubuc, and K. Grenier, "A microwave and microfluidic planar resonator for efficient and accurate complex permittivity characterization of aqueous solutions," *IEEE Trans. Microw. Theory Techn.*, vol. 61, no. 2, pp. 972–978, Feb. 2013.
[48] A. Salim, S.-H. Kim, J. Y. Park, and S. Lim, "Microfluidic biosensor based on microwave substrate-integrated waveguide cavity resonator," *J. Sensors*, vol. 2018, pp. 1–13, Feb. 2018.
[49] M. H. Zarifi, H. Sadabadi, S. H. Hejazi, M. Daneshmand, and A. Sanati-Nezhad, "Noncontact and nonintrusive microwave-microfluidic flow sensor for energy and biomedical engineering," *Sci. Rep.*, vol. 8, no. 1, pp. 1–10, Dec. 2018.
[50] J. Castillo-León, and W. E. Svendsen, *Lab-on-a-Chip Devices and Micro-Total Analysis Systems: A Practical Guide*. New York, NY, USA: Springer, 2014.
[51] J. Munoz-Enano, P. Velez, L. Su, M. Gil-Barba, and F. Martin, "A reflective-mode phase-variation displacement sensor," *IEEE Access*, vol. 8, pp. 189565–189575, Oct. 2020.
[52] A. K. Jha, A. Lamecki, M. Mrozowski, and M. Bozzi, "A highly sensitive planar microwave sensor for detecting direction and angle of rotation," *IEEE Trans. Microw. Theory Techn.*, vol. 68, no. 4, pp. 1598–1609, Apr. 2020.
[53] A. K. Horestani, Z. Shaterian, and F. Martin, "Rotation sensor based on the cross-polarized excitation of split ring resonators (SRRs)," *IEEE Sensors J.*, vol. 20, no. 17, pp. 9706–9714, Sep. 2020.
[54] A. Velez, F. Aznar, J. Bonache, M. C. Velazquez-Ahumada, J. Martel, and F. Martin, "Open complementary split ring resonators (OCSRRs) and their application to wideband CPW band pass filters," *IEEE Microw. Wireless Compon. Lett.*, vol. 19, no. 4, pp. 197–199, Apr. 2009.
[55] D. M. Pozar, *Microwave Engineering*, 4th ed. Hoboken, NJ, USA: Wiley, 2011.
[56] J. Coromina, J. Munoz-Enano, P. Velez, A. Ebrahimi, J. Scott, K. Ghorbani, and F. Martin, "Capacitively-loaded slow-wave transmission lines for sensitivity improvement in phase-variation permittivity sensors," in *Proc. 50th Eur. Microw. Conf. (EuMC)*, Utrecht, The Netherlands, Jan. 2021, pp. 491–494.
[57] A. Ebrahimi, J. Coromina, J. Muñoz-Enano, P. Vélez, J. Scott, K. Ghorbani, and F. Martín, "Highly sensitive phase-variation dielectric constant sensor based on a capacitively-loaded slow-wave transmission line," *IEEE Trans. Circuit Syst.*, submitted for publication.
[58] F. Martín, *Artificial Transmission Lines for RF and Microwave Applications*. Hoboken, NJ, USA: Wiley, 2015.
[59] S. Mohammadi, B. Wiltshire, M. C. Jain, A. V. Nadaraja, A. Clements, K. Golovin, D. J. Roberts, T. Johnson, I. Foulds, and M. H. Zarifi, "Gold coplanar waveguide resonator integrated with a microfluidic channel for aqueous dielectric detection," *IEEE Sensors J.*, vol. 20, no. 17, pp. 9825–9833, Sep. 2020.
[60] S. Harnsoongnoen and A. Wanthong, "A non-contact planar microwave sensor for detection of high-salinity water containing NaCl, KCl, $CaCl_2$, $MgCl_2$ and Na_2CO_3," *Sens. Actuators B, Chem.*, vol. 331, Mar. 2021, Art. no. 129355.
[61] A. K. Jha, A. Lamecki, M. Mrozowski, and M. Bozzi, "A microwave sensor with operating band selection to detect rotation and proximity in the rapid prototyping industry," *IEEE Trans. Ind. Electron.*, vol. 68, no. 1, pp. 683–693, Jan. 2021.
[62] M. Durán-Sindreu, F. Aznar, A. Vélez, J. Bonache, and F. Martín, "Analysis and applications of OSRR- and OCSRR-loaded transmission lines: A new path for the design of compact transmission line metamaterials," *Metamaterials*, vol. 4, nos. 2–3, pp. 139–148, Aug. 2010.
[63] M. Abdolrazzaghi, M. Daneshmand, and A. K. Iyer, "Strongly enhanced sensitivity in planar microwave sensors based on metamaterial coupling," *IEEE Trans. Microw. Theory Techn.*, vol. 66, no. 4, pp. 1843–1855, Apr. 2018.
[64] M. Abdolrazzaghi and M. Daneshmand, "Exploiting sensitivity enhancement in micro-wave planar sensors using intermodulation products with phase noise analysis," *IEEE Trans. Circuits Syst. I, Reg. Papers*, vol. 67, no. 12, pp. 4382–4395, Dec. 2020.

LIJUAN SU (Member, IEEE) was born in Qianjiang (Hubei), China, in 1983. She received the B.S. degree in communication engineering and the M.S. degree in circuits and systems from the Wuhan University of Technology, Wuhan, China, in 2005 and 2013 respectively, and the Ph.D. degree in electronic engineering from the Universitat Autonoma de Barcelona, Barcelona, Spain, in 2017. From November 2017 to December 2019, she worked as a Postdoc Researcher in Flexible Electronics Research Center, Huazhong University of Science and Technology, Wuhan, China. She is currently a Postdoc Researcher with CIMITEC, Universitat Autonoma de Barcelona, Spain. Her current research interests focus on the development of novel microwave sensors with improved performance for biosensors, dielectric characterization of solids and liquids, defect detection, and industrial processes.

JONATHAN MUÑOZ-ENANO (Graduate Student Member, IEEE) was born in Mollet del Vallès (Barcelona), Spain, in 1994. He received the bachelor's degree in electronic telecommunications engineering and the master's degree in telecommunications engineering from the Autonomous University of Barcelona (UAB), in 2016 and 2018, respectively. Actually, he is working in the same university in the elaboration of his Ph.D., which is focused on the development of microwave sensors based on metamaterials concepts for the dielectric characterization of materials and biosensors.

PARIS VÉLEZ (Member, IEEE) was born in Barcelona, Spain, in 1982. He received the degree in telecommunications engineering, specializing in electronics, the electronics engineering degree, and the Ph.D. degree in electrical engineering from the Universitat Autònoma de Barcelona, Barcelona, in 2008, 2010, and 2014, respectively. His Ph.D. thesis concerned common mode suppression differential microwave circuits based on metamaterial concepts and semi-lumped resonators. During the Ph.D., he was awarded with a pre-doctoral teaching and research fellowship by the Spanish Government from 2011 to 2014. From 2015 to 2017, he was involved in the subjects related to metamaterials sensors for fluidics detection and characterization at LAAS-CNRS through a TECNIOSpring fellowship cofounded by the Marie Curie program. His current research interests include the miniaturization of passive circuits RF/microwave and sensors-based metamaterials through Juan de la Cierva fellowship. He is a Reviewer for the IEEE TRANSACTIONS ON MICROWAVE THEORY AND TECHNIQUES and for other journals.

MARTA GIL-BARBA (Member, IEEE) was born in Valdepeñas, Ciudad Real, Spain, in 1981. She received the physics degree from Universidad de Granada, Spain, in 2005, and the Ph.D. degree in electronic engineering from the Universitat Autònoma de Barcelona, Barcelona, Spain, in 2009. She studied one year with the Friedrich Schiller Universität Jena, Jena, Germany. During her Ph.D. Thesis, she was holder of a METAMORPHOSE NoE grant and National Research Fellowship from the FPU Program of the Education and Science Spanish Ministry. As a postdoctoral researcher, she was awarded with a Juan de la Cierva fellowship working in the Universidad de Castilla-La Mancha. She was a Postdoctoral Researcher with the Institut für Mikrowellentechnik und Photonik in Technische Universität Darmstadt and in the Carlos III University of Madrid. She is currently an Associate Professor with the Universidad Politécnica de Madrid. She has worked in metamaterials, piezoelectric MEMS, and microwave passive devices. Her current interests include metamaterials sensors for fluidic detection.

PAU CASACUBERTA was born in Sabadell (Barcelona), Spain, in 1997. He received the bachelor's degree in electronic telecommunications engineering and the bachelor's degree in computer engineering in 2020 from the Universitat Autònoma de Barcelona (UAB), where he is currently pursuing the master's degree in telecommunications engineering. He received the Collaboration fellowship by the Spanish Government in 2019 for developing his Bachelor's Thesis in highly sensitive microwave sensors based in stepped impedance structures.

FERRAN MARTIN (Fellow, IEEE) was born in Barakaldo (Vizcaya), Spain, in 1965. He received the B.S. degree in physics from the Universitat Autònoma de Barcelona (UAB), in 1988, and the Ph.D. degree in 1992. From 1994 to 2006, he was an Associate Professor in electronics with the Departament d'Enginyeria Electrònica (Universitat Autònoma de Barcelona), and since 2007, he is a Full Professor of electronics. In recent years, he has been involved in different research activities including modeling and simulation of electron devices for high frequency applications, millimeter wave and THz generation systems, and the application of electromagnetic bandgaps to microwave and millimeter wave circuits. He is now very active in the field of metamaterials and their application to the miniaturization and optimization of microwave circuits and antennas. Other topics of interest include microwave sensors and RFID systems, with special emphasis on the development of high data capacity chipless-RFID tags. He is the Head of the Microwave Engineering, Metamaterials and Antennas Group (GEMMA Group) at UAB, and the Director of CIMITEC, a research Center on Metamaterials supported by TECNIO (Generalitat de Catalunya). He has organized several international events related to metamaterials and related topics, including Workshops at the IEEE International Microwave Symposium (years 2005 and 2007) and European Microwave Conference (2009, 2015 and 2017), and the Fifth International Congress on Advanced Electromagnetic Materials in Microwaves and Optics (Metamaterials 2011), where he acted as Chair of the Local Organizing Committee. He has acted as Guest Editor for six Special Issues on metamaterials and sensors in five International Journals. He has authored or coauthored over 650 technical conference, letter, journal papers and book chapters, he is co-author of the book on Metamaterials entitled *Metamaterials with Negative Parameters: Theory, Design and Microwave Applications* (John Wiley & Sons Inc.), author of the book *Artificial Transmission Lines for RF and Microwave Applications* (John Wiley & Sons Inc.), co-editor of the book *Balanced Microwave Filters* (Wiley/IEEE Press), and co-author of the book *Time-Domain Signature Barcodes for Chipless-RFID and Sensing Applications* (Springer). He has generated 21 PhDs, has filed several patents on metamaterials and has headed several Development Contracts.

Dr. Martín is a member of the IEEE Microwave Theory and Techniques Society (IEEE MTT-S). He is reviewer of the IEEE TRANSACTIONS ON MICROWAVE THEORY AND TECHNIQUES and the IEEE MICROWAVE AND WIRELESS COMPONENTS LETTERS, among many other journals, and he serves as member of the Editorial Board of *IET Microwaves, Antennas and Propagation, International Journal of RF and Microwave Computer-Aided Engineering, and Sensors*. He is also a member of the Technical Committees of the European Microwave Conference (EuMC) and International Congress on Advanced Electromagnetic Materials in Microwaves and Optics (Metamaterials). Among his distinctions, he has received the 2006 Duran Farell Prize for Technological Research, he holds the *Parc de Recerca UAB—Santander* Technology Transfer Chair, and he has been the recipient of three ICREA ACADEMIA Awards (calls 2008, 2013 and 2018). He is a Fellow of the IET.